NAVAL POSTGRADUATE SCHOOL
Monterey, California

THESIS

INVESTIGATION OF DEEP DIELECTRIC CHARGING
AND SUBSEQUENT CURRENTS
ON
GEOSYNCHRONOUS SPACECRAFT

by

Donald S. Smith

December, 1991

Thesis Advisor: R. C. Olsen

REPORT DOCUMENTATION PAGE

1a REPORT SECURITY CLASSIFICATION Unclassified		1b RESTRICTIVE MARKINGS
2a SECURITY CLASSIFICATION AUTHORITY		3 DISTRIBUTION/AVAILABILITY OF REPORT Approved for public release; distribution is unlimited.
2b DECLASSIFICATION/DOWNGRADING SCHEDULE		
4 PERFORMING ORGANIZATION REPORT NUMBER(S)		5 MONITORING ORGANIZATION REPORT NUMBER(S)

6a NAME OF PERFORMING ORGANIZATION Naval Postgraduate School	6b OFFICE SYMBOL (If applicable) Code 33	7a NAME OF MONITORING ORGANIZATION Naval Postgraduate School
6c ADDRESS (City, State, and ZIP Code) Monterey, CA 93943-5000		7b ADDRESS (City, State, and ZIP Code) Monterey, CA 93943-5000
8a NAME OF FUNDING/SPONSORING ORGANIZATION	8b OFFICE SYMBOL (If applicable)	9 PROCUREMENT INSTRUMENT IDENTIFICATION NUMBER
8c ADDRESS (City, State, and ZIP Code)		10 SOURCE OF FUNDING NUMBERS

	Program Element No	Project No	Task No	Work Unit Accession Number

11 TITLE (Include Security Classification)

INVESTIGATION OF DEEP DIELECTRIC CHARGING AND SUBSEQUENT CURRENTS ON GEOSYNCHRONOUS SPACECRAFT

12 PERSONAL AUTHOR(S) Smith, Donald S.

13a TYPE OF REPORT Master's Thesis	13b TIME COVERED From To	14 DATE OF REPORT (year, month, day) December 1991	15 PAGE COUNT 94

16 SUPPLEMENTARY NOTATION

The views expressed in this thesis are those of the author and do not reflect the official policy or position of the Department of Defense or the U.S. Government.

17 COSATI CODES			18 SUBJECT TERMS (continue on reverse if necessary and identify by block number)
FIELD	GROUP	SUBGROUP	Spacecraft Charging, Differential Charging, Surface Charging, Deep Dielectric Charging, Potential Barriers, ISEE 1, SCATHA

19 ABSTRACT (continue on reverse if necessary and identify by block number)

Deep dielectric charging is the suspected mechanism for formation of potential barriers aboard the ISEE 1 spacecraft. Energetic electron distribution functions in the plasmasheet were examined for both surface and deep dielectric charging. Surface charging was found to dependent on whether the satellite surfaces were in shadow. The surface potential is regulated by photoelectric emission, and is two orders of magnitude higher than other mechanisms. Deep dielectric charging deposits charge within dielectrics, and is independent of surface effects, such as photoemission and radiation-induced conductivity. Deposition of electrons into solar array cover cells begins at approximately 10 keV.

20 DISTRIBUTION/AVAILABILITY OF ABSTRACT ☒ UNCLASSIFIED/UNLIMITED ☐ SAME AS REPORT ☐ DTIC USERS	21 ABSTRACT SECURITY CLASSIFICATION Unclassified	
22a NAME OF RESPONSIBLE INDIVIDUAL R. C. Olsen	22b TELEPHONE (Include Area code) (408) 646 2019	22c OFFICE SYMBOL PH/OS

DD FORM 1473, 84 MAR   83 APR edition may be used until exhausted   SECURITY CLASSIFICATION OF THIS PAGE
                                 All other editions are obsolete   UNCLASSIFIED

Investigation of Deep Dielectric Charging
and Subsequent Currents
on
Geosynchronous Spacecraft

by

Donald S. Smith
Captain, United States Marine Corps
B.S., University of Utah, 1983

Submitted in partial fulfillment
of the requirements for the degree of

MASTER OF SCIENCE IN PHYSICS

from the

NAVAL POSTGRADUATE SCHOOL
DECEMBER 1991

ABSTRACT

Deep dielectric charging is the suspected mechanism for formation of potential barriers aboard the ISEE 1 spacecraft. Energetic electron distribution functions in the plasmasheet were examined for both surface and deep dielectric charging. Surface charging was found to be dependent on whether the satellite surfaces were in shadow. The surface potential is regulated by photoelectric emission, and is two orders of magnitude higher than other mechanisms. Deep dielectric charging deposits charge within dielectrics, and is independent of surface effects, such as photoemission and radiation-induced conductivity. Deposition of electrons into solar array cover cells begins at approximately 10 keV.

TABLE OF CONTENTS

ACKNOWLEDGEMENTS

I am indebted to Professor Olsen for his help in the development of this thesis, particularly for his encouragement, insight, and patience in answering many questions. I also would like to thank Professor Maruyama who was instrumental in explaining the concept of radiation-induced conductivity.

A special note of thanks to my family who endured late hours, no Dad, and relentless requests for quiet.

I. INTRODUCTION

This thesis will examine spacecraft charging and, in particular, deep dielectric charging. Spacecraft charging is an important consideration in operating satellites in a plasma environment. A build-up of charge on the surface and within dielectric materials is identified with abnormal system behavior. These anomalies have been linked with unexpected system resets, false signals, and even total satellite failure.

Theoretical calculations of energetic electron fluxes will be compared to observed in-situ data, to determine if charged particles present have sufficient energy to cause deep dielectric charging. The particle energy level for which differential charging begins will also be investigated.

In subsequent chapters, the structure and characteristics of the magnetosphere will be explored. Several different electron distribution functions are used to describe the ambient plasma and how it effects surface and deep dielectric charging of satellites. Radiation-induced conductivity can alter the characteristics of exposed dielectrics, which in turn, can effect the re-distribution of deposited charge. Contributions to the

charging process by different mechanisms vary by several
orders of magnitude. Comparisons will show which are
important, and those that can be ignored. Finally, a
correlation will be made between the calculated integral
flux and data from geosynchronous satellite charging events.

II. BACKGROUND

A. Environment

The earth is subject to a magnetized flow of plasma
called the solar wind (Figure 1). Interruption of the solar
wind flow around the earth, by the earth's magnetic field
forms a structure called the magnetosphere. Within the
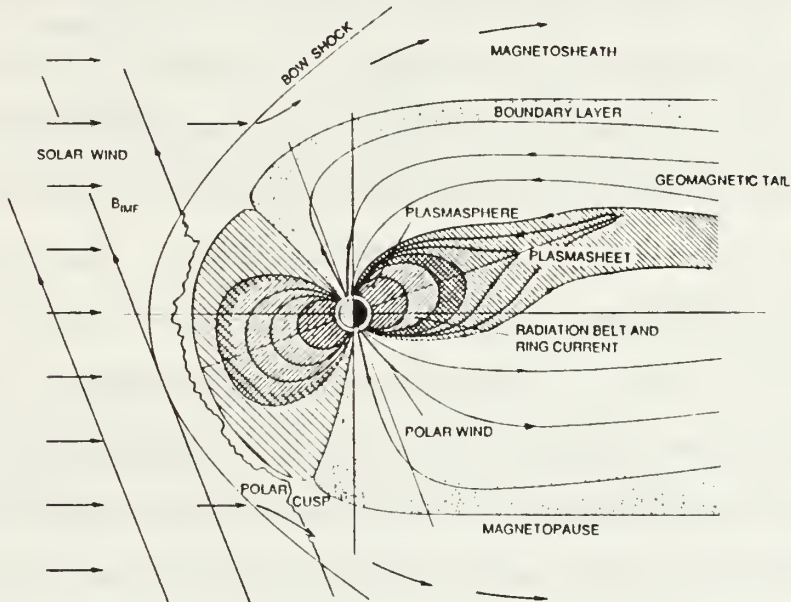magnetosphere are several components which comprise its

Figure 1

[Ref 1]

infrastructure. The magnetopause separates the earth's
magnetic field from the solar wind. Inside the

3

magnetosphere is the plasmasheet. Inward of the plasmasheet
is the plasmasphere. The plasmasphere exists as a non-
uniform dipolar region, centered on the earth's north-south
axis.

Satellites pass through three main regions daily while
in geosynchronous orbit. On the day side, from 1200 to 1600
local time (LT), the satellite is generally between the
plasmasphere and the magnetosheath, in a region populated by
the remnants of convected plasmasheet electrons, and ion and
electron flows out of the ionosphere (re-filling). In this
region, the spacecraft will transit a cool, dense plasma,
and be continually in sunlight. At 1600 (LT) the satellite
will move into the plasmapause, the region separating the
plasmasphere from the plasmasheet, or on very quiet days,
into the dusk bulge of the plasmasphere. The plasmasheet
can inject energetic particles into this boundary region,
raising the overall temperature of the plasma. By 2000 LT
the spacecraft typically enters the plasmasheet, an area of
energetic particles, and remains in this region until 0800
LT. The hot plasma encountered (several KeV) encourages
vehicle charging. One of the results of the charging is
anomalies. Anomalies are erroneous satellite functions that
are generated by the re-distribution of charge deposited by
the plasma. These system upsets cause a wide range of
electrical problems, including, in severe cases, satellite
failure. Anomalies will be discussed in greater detail

4

later in this section. By 0800 LT, the electron temperature
has dropped, as the plasmasheet electrons drift sunward.
The probability of satellite charging drops rapidly as the
satellite moves into the day side. Table 1 summarizes the
composition and characteristics of the magnetospheric

TABLE 1

Region	L_{min}	L_{max}	e^-/cm^3	Energies(eV)
Plasmasphere	.2	4	$10-10^3$	.1 - 1.0
Plasmasheet	8	30	.1-10	$10^3 - 4x10^4$

plasma   [Ref 1, p. 2-14 to 2-35, Ref 2, p. 3681 to 3691, Ref
3, p. 7 to 11, p. 81 to 85].

The magnetosphere is populated with charged particles
via diffusion/acceleration from the ionosphere and perhaps
the solar wind. At quiet times, the outer plasmasphere can
move out to include geosynchronous orbit [Ref 4, p. 3587 to
3611]. During magnetic substorms, injections of 10 KeV to
several MeV electrons from the plasmasheet are observed at
geosynchronous altitude. It is thought the infusion of
these energetic electrons is responsible for spacecraft
charging [Ref 5, p. 278 to 308, Ref 6, p. 4-1 to 4-16].

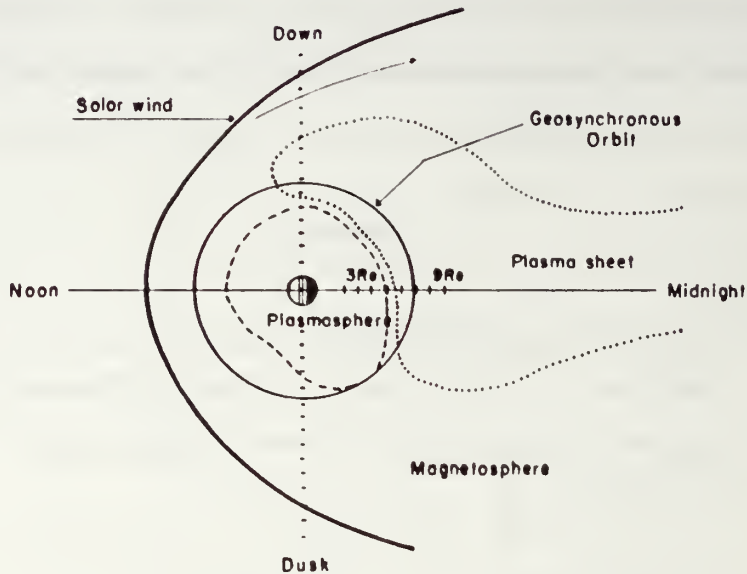Figure 2 summarizes the movement of the regions at
geosynchronous altitude.

Figure 2

B. Spacecraft Charging

Spacecraft charging is a phenomena observed when a
spacecraft interacts with any plasma. The result of this
interaction is an accumulation of charge within the body of
the satellite as well as a buildup on the surface. The
accumulation of charge on a spacecraft appears in two
distinct ways. Absolute charging is where the potential of
the entire spacecraft changes with respect to the ambient
plasma. The uniform change in potential, with respect to
the plasma will not, in general, effect the onboard

6

electronic systems. Differential charging is where dielectric surfaces of the spacecraft are charged to different potentials relative to each other. A significant result of differential charging is strong local electric fields on the surface and within the body of the satellite. These electric fields give rise to the possibility of damaging electrical discharges [Ref 1, p. 2-1 to 2-3].

1. Surface Charging

Surface charging is the buildup of charge on the surface of a satellite from its interaction with the plasma environment. The phenomena of large negative potentials was first recognized in the early 1970's from data taken by the Applied Technology Satellite (ATS) 5 [Ref 7, p. 561 to 569]. Surface charging at geosynchronous orbit typically reaches several hundred volts negative in sunlight, and to more than -10^4 volts in eclipse. The potentials vary with the environment, on very short time scales ($\tau < 1$ second) in eclipse, longer in sunlight [Ref 8, p. 5657 to 5667, Ref 9, p. 263 to 276].

There have been historically many instances of satellite charging. Deforest showed a correspondence between injections of energetic plasma from magnetic substorms and large negative potentials on Applied Technology Satellite (ATS) 5 when the spacecraft was in eclipse [Ref 7, p. 651 to 659, Ref 4, p. 3587 to 3611]. ATS

5 was found to charge to potentials of -5 to -10 kV in eclipse, and later, ATS 6 was found to charge to similar potentials in eclipse. In Figure 3, the charging of ATS 6 in eclipse is illustrated. Electron and ion counts at 18.4 keV are shown, along with the potential. The injection of hot plasma at approximately 21:23 UT is signalled by the increase in the 18.4 keV electron flux. The response of the satellite is to charge to approximately -6 kV in less than one minute. This illustrates the short time scale associated with charging of the satellite frame (The satellite capacitance to space is relatively small).
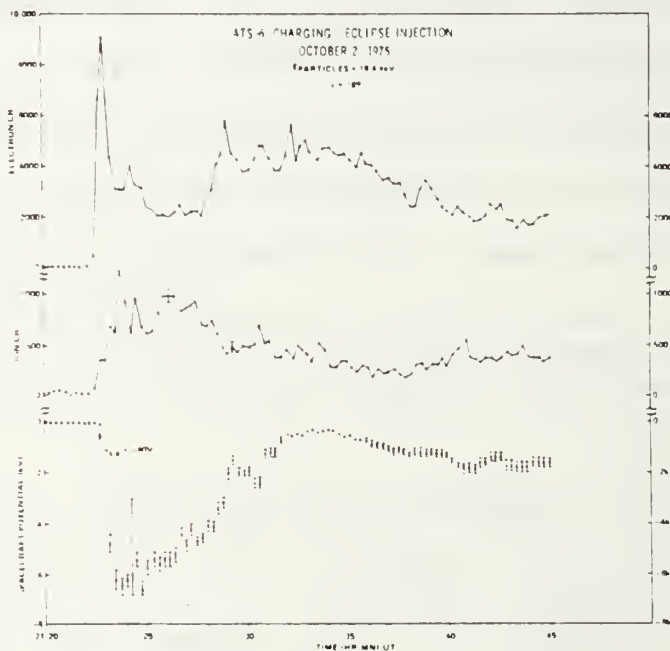

Figure 3

[Ref 22]

On 8 October, 1975, ATS 6 charged to a record negative potential, to 19 kV in eclipse [Ref 10, p. 362 to 366].

8

ATS 5 and 6 both charged to negative potentials in sunlight. This was uncommon for ATS 5, but the satellite did reach a potential of -400 V on one occasion [Ref 8, p. 5657 to 5667]. ATS 6 reached -1.5 kV [Ref 10, p. 362 to 366]. Figure 4 shows that the time scale for sunlight charging is much longer than for charging in eclipse. Here the injection of hot plasma occurs at approximately 0800, but the satellite potential does not peak for almost an hour. The subsequent decline in potential is associated with the cooling of the ambient plasma.
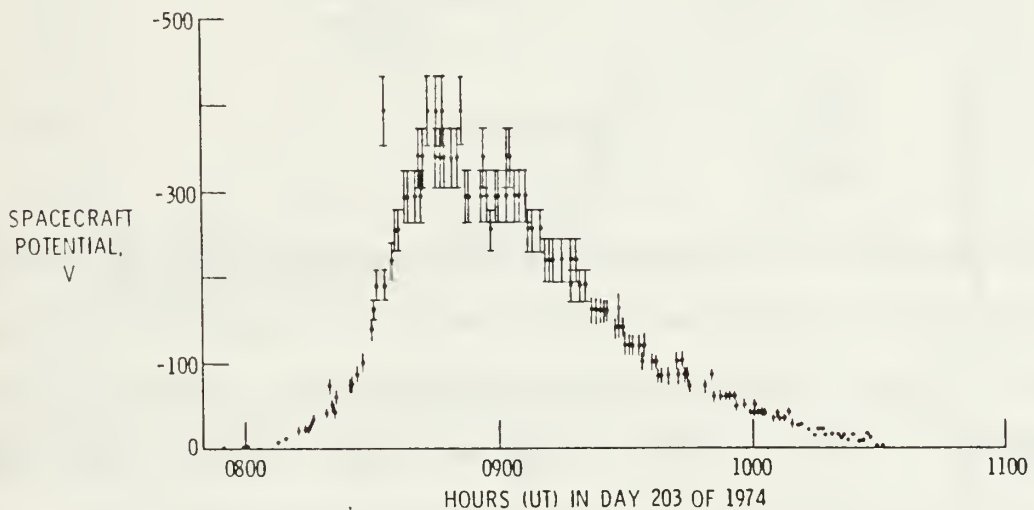
ATS-6 POTENTIAL: CHARGING IN SUNLIGHT

Figure 4

[Ref 22]

Reasoner et al., did a statistical study of 40 days of ATS 6 charging in daylight. The study revealed that the

9

probability of charging was over 50% during the local
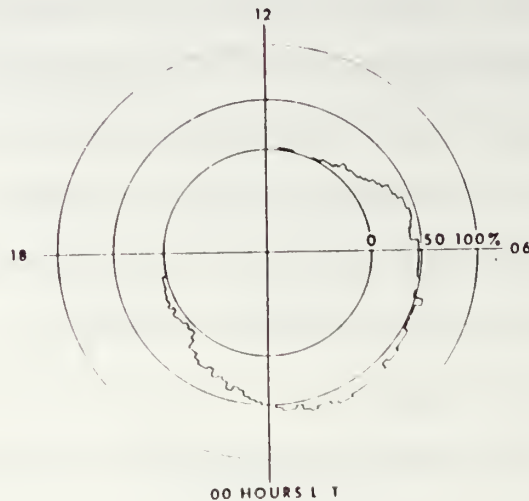midnight to dawn sector as shown by Figure 5 [Ref 11, p. 89
to 101].

Figure 5

Additionally, in a survey of high energy charging events on
the near-geosynchronous P78-2 satellite (SCATHA), Mullen et
al., found a statistical distribution for charging events
that occurred between 1900 LT and 0900 LT. The charging
occurred from 5.5 to 7.7 R_E. It was also shown that
spacecraft potentials correlate to electron fluxes
with energies of 30 keV or more [Ref 12, p. 1474 to 1490].
        The International Sun Earth Explorer (ISEE) 1
spacecraft was built to electrostatic cleanliness

specifications which it was thought would prevent daylight

charging. However, ISEE 1 did charge to significant

negative potentials (~ -100 V) in sunlight while near

geosynchronous orbit in March, 1978 [Ref 13, p. 5568 to

5578]. This charging event motivates the work done here.

Figure 6 shows a charging event on 17 March, 1979 on board

ISEE 1 [Ref 13, p. 5568 to 5578]. Note that the time scale

is over 4 hours. This is 4 to 5 times as long as the
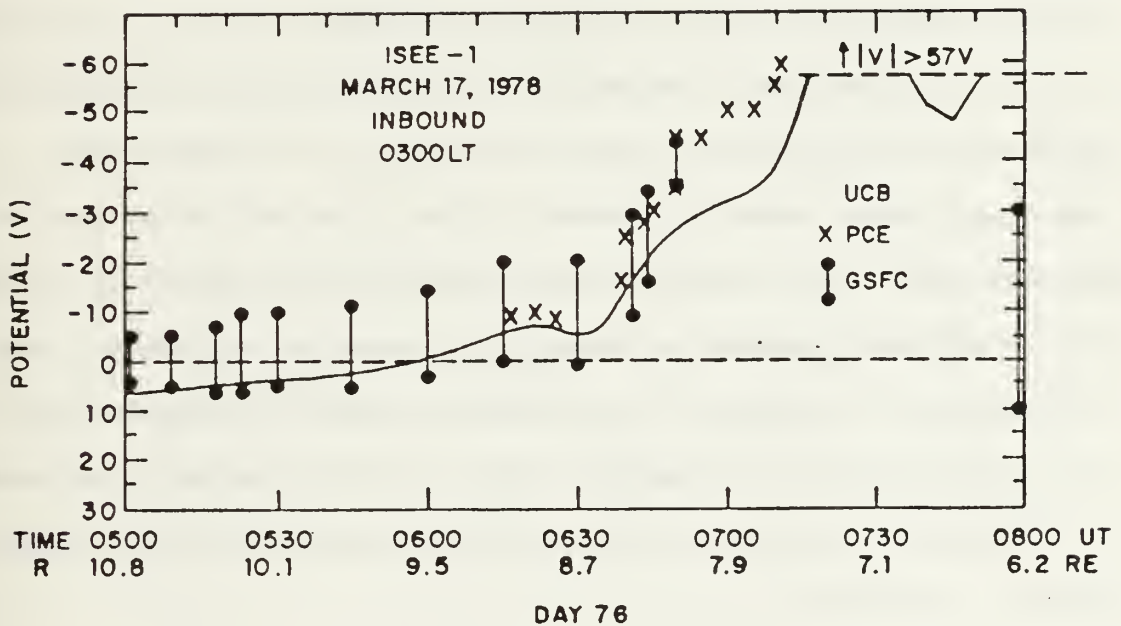
charging period that Figure 4 shows.

Figure 6

[Ref 13]

Away from geosynchronous orbit, satellite charging

occurred on the Defense Meteorological Satellite Program

11

(DMSP) satellite while flying through auroral regions. Negative potentials from 50 V to 1.5 kV were observed while the satellite crossed high magnetic latitudes in low earth orbit (LEO) [Ref 14, manuscript].

2. Differential Charging

Differential Charging is the charging of a piece of a spacecraft relative to an adjacent section. Differential charging occurs, in general, because of variations in materials, shadowing of surfaces, and the deposition of charge into dielectrics. There are a variety of materials used for satellite surfaces, many of which are non-conductors (dielectrics), such as kapton, teflon, and glass.

Photons from the sun incident on a spacecraft cause electrons to be emitted from the surface, provided the energy of each photon is greater than the work function of the material. Because of this shadowing is important. The nature of such shadowing depends on satellite geometry and stabilization technique. The most popular techniques are three-axis and spin stabilization. In the latter case, the orientation of the spin axis relative to the sun-satellite line is important.

As previously mentioned, surface charging in eclipse can reach kilovolt potentials, while the satellite potential in sunlight is generally not as large [Ref 8, p. 5657 to 5667]. Shadowed dielectrics will behave as though they are in eclipse, and charge to much larger negative potentials than the satellite frame or illuminated dielectrics. A potential gradient of kV/cm across dielectrics can lead to arcs and electrical discharges if the accompanying electric fields exceed the dielectric breakdown strength [Ref 5, p. 277 to 308].

The effects of differential charging have been observed. ATS 6 data revealed evidence of differential charging. Figure 7 shows an electron distribution observed by ATS 6. [Ref 15, p. 715 to 719]. This figure shows that electrons with energy below 50 eV must have been generated on or near the satellite surface. Hence, the photoelectrons and secondary electrons generated on the satellite surface were being reflected by some form of barrier, and were unable to escape the vehicle. Otherwise, astronomical values for the plasma density result. Olsen et al.,

postulated the barrier was caused by differential charging

vice electron space charge [Ref 16, p. 6809 to 6819].

Electron Distribution Function
Sept 30, 1974   0609 UT

$\phi_{sat} \equiv -2000$ V
(in eclipse)

$T \equiv 6$ eV
$n \equiv 0.4$ cm^{-3} if Secondaries
$n > 10^{99}$ cm^{-3} if Ambient

$T \equiv 320$ eV
$n \equiv 17$ cm^{-3}

Transition Energy $\equiv$
50 eV

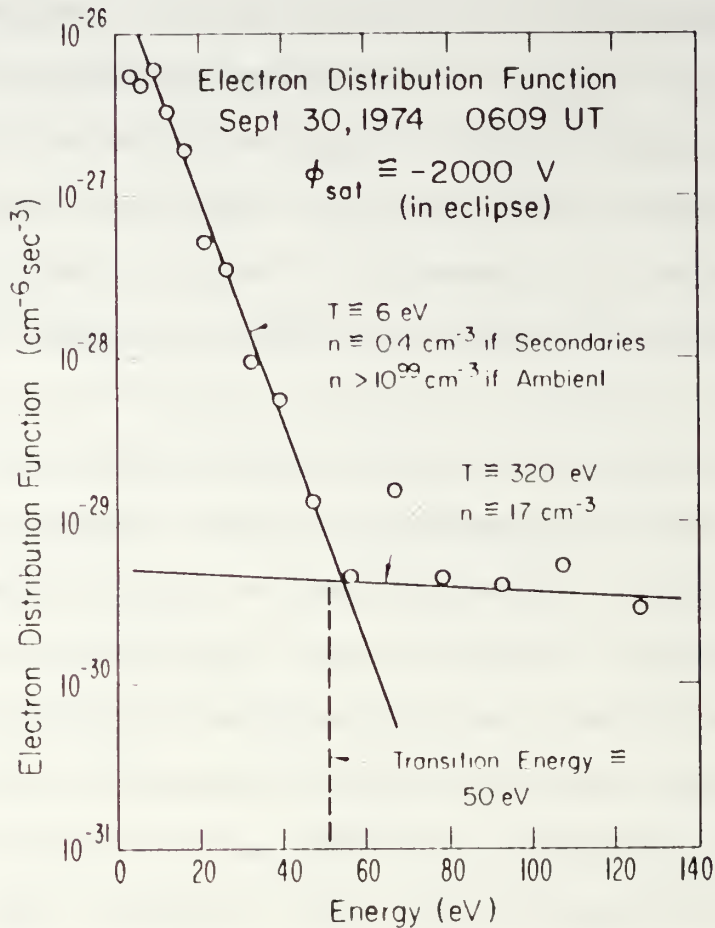Electron Distribution Function (cm^{-6}sec^{-3})

Energy (eV)

Figure 7

Differential charging of dielectrics could be
directly measured with the satellite surface potential
monitor (SSPM) on the SCATHA satellite. Dielectric
materials (kapton, teflon, SiO$_2$) were found to charge to

14

negative kilovolt potentials when shadowed as shown in
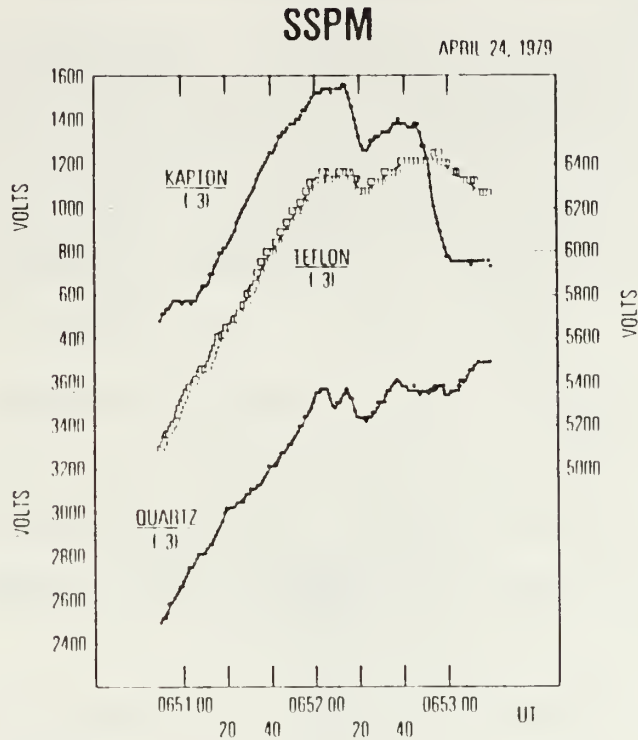Figure 8.

SSPM

APRIL 24, 1979

Figure 8

[Ref 18]

This differential charging occurred with a time
constant of tens of seconds, as appropriate to the
capacitance associated with the thin dielectrics. This is
in contrast to the more rapid charging of the satellite as a
whole (τ < 1 second), which has a relatively lower
capacitance to space [Ref 18, p. 506 to 509]. The
differential charging is also responsible for the charging
of the vehicle as a whole [Ref 17, p. 14-1 to 14-12].
Modelling of daylight charging showed that the barrier

15

induced by differential charging allowed a net negative current to the sunlit surfaces.

C. Anomalies

The magnetosphere is often an unfriendly environment in which satellites must survive and operate. Spacecraft are subjected to high energy particle fluxes, and discharges resulting from surface and differential charging can produce electromagnetic pulses (EMP). These EMP can enter into the internal circuitry through unshielded cables, ungrounded components, and any external conduit that will transport the Fourier spectra of the EMP. Additionally, very high energy particles can cause single event upsets (SEU) [Ref 1, p. 4-22 to 4-23].

Satellite anomalies were attributed to charging following the realization in the mid-1970's that large negative potentials could be found on satellites positioned at 6.6 earth radii. Figure 9 shows a distribution of anomalies as a function of time of day for several geostationary spacecraft. This historical figure was promptly related to the charging distribution obtained from ATS 6 (see Figure 5) and a correspondence was suggested [Ref 11, p. 89 to 101].

A variety of anomalies for several different satellites are tabulated in Reference 1. They include power-on resets,

EMP, spin-up, false flags in software, clock shifts, false
or phantom commands, telemetry errors, power-downs,
circuit noise, power system shutdowns, system upsets, and
total satellite failures. The figure is a distribution of
anomalies observed on several geosynchronous satellites.
The times are local and the distance from the origin is
solely to allow visual resolution of the events [Ref 1, p.
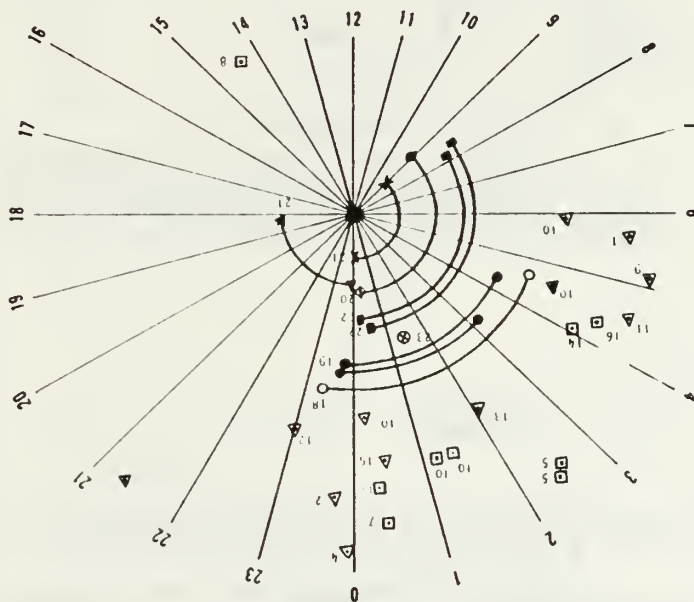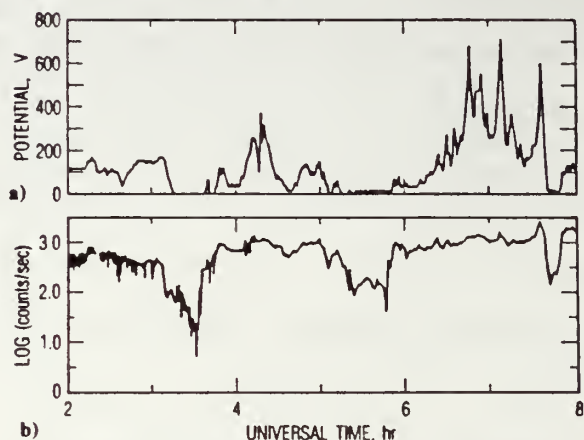5-2 to 5-11].

Figure 9

[Ref 11]

Although there are many examples of anomalies in
geosynchronous satellites, most are difficult to relate
unambiguously to satellite charging as a cause. The most
revealing case was with the SCATHA satellite on 22
September, 1982, when differential charging, EMPs, and

17

anomalies were found together as shown in Figure 10 [Ref 19, p. 239 to 243].

a) The absolute value of the voltage on the Satellite Surface Potential Monitor gold sample as a function of time. The potential of the sample is negative with respect to the ground reference; b) the count rate for 18.4 keV electrons as a function of time.
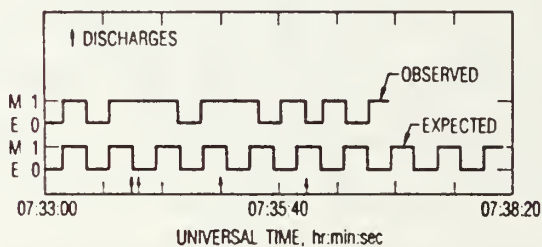
The timing sequence of the antenna switch on the VLF Analyzer experiment during one time period when anomalous behavior occurred on September 22, 1982.

Figure 10

During a period of energetic electron flux and high surface potentials, the timing sequence of a switch in an

experimental package showed anomalous behavior. The arrows
at the bottom of the figure show a flip in logic states
coinciding with discharge events.

An example from a completely different environment, the
Jovian magnetosphere, provides an unusually clear
demonstration of the relationship between anomalies and an
environmental cause. A sequence of anomalies occurred when
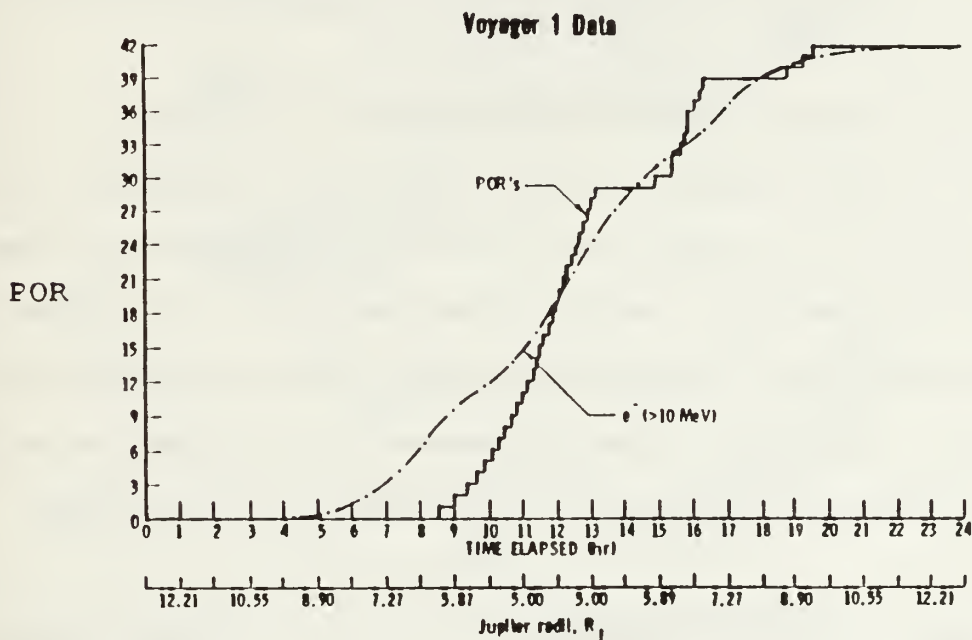Voyager I passed Jupiter on 5 March, 1979, as seen in Figure
11.

Figure 11

[Ref 20]

Prior to and during the fly-by at 5 R_J, a series of
power-on resets (POR) plagued a critical photographic
sequence. Figure 11 shows resets and the energetic electron
flux. There is a clear correspondence [Ref 20, p. 21 to
30].

Laboratory simulation of the POR process identified unterminated spare leads in a cable bundle in which the POR cable co-existed. A portion of this cable exited the spacecraft body and was exposed to the plasma environment. Re-creation of the observed environment produced 25 mA current pulses capable of inducing the POR. Surface charging in a cold dense plasma was ruled out and a correspondence was established between the POR and the 10 MeV e⁻ flux component measured by on-board instruments [Ref 20, p. 21 to 30].

This example shows the importance of energetic electrons, the universality of spacecraft charging, and anomalies. It is also one of the prime examples of deep dielectric charging, which is the deposition of charge into dielectrics (like cable insulation) where the charge is trapped, accumulates, and ultimately is released as an EMP. Deep dielectric charging is the primary focus of this thesis.

Reagan et al., were among the first to discuss deep dielectric charging (Figure 12). They presented SCATHA data for days with large fluxes of high energy electrons (several MeV) and found a correspondence to charging. Energetic electrons incident on satellite surfaces can bury themselves either into dielectric materials or into floating metal (conductors not connected to the spacecraft ground). As charge builds up within the satellite body, it may exceed

20

the breakdown strength of the material and arc. The

associated EMP may be sufficiently large to induce anomalous

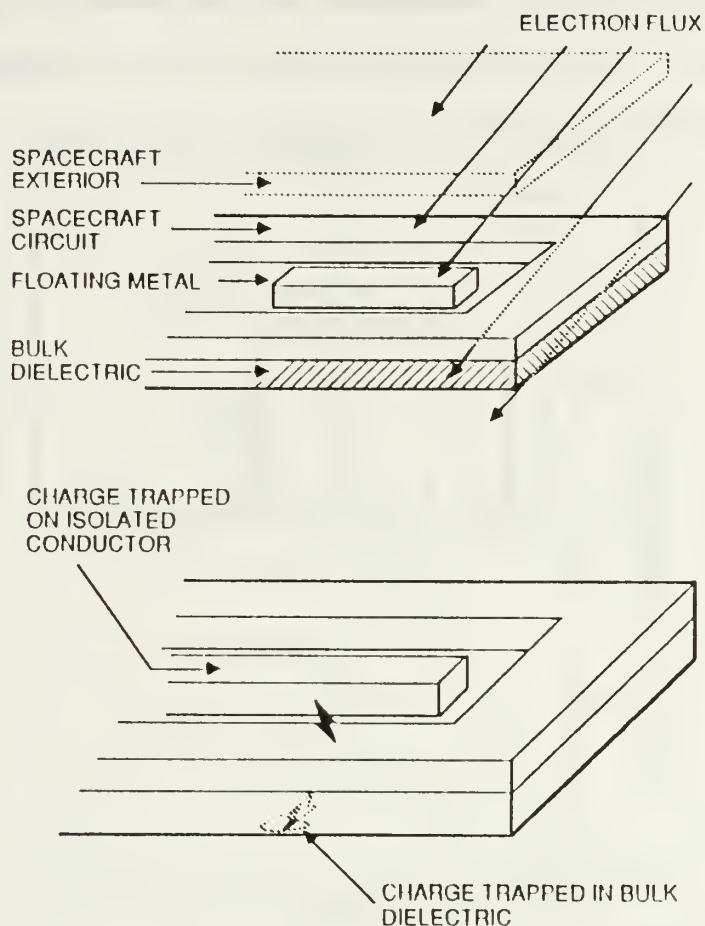behavior in one or more of the satellite electronic

components.

Figure 12

[Ref 1]

The deposition and buildup of charge in the dielectric

were modelled and found in agreement with in situ

measurements. Although peak electric field strength was

below material breakdown levels, rapid changes in these fields resulted in large EMP [Ref 21, p. 354 to 365].

Baker et al., have also looked at the consequences of high energy electron fluxes. Figure 13 shows a connection between high energy electrons at geosynchronous orbit (measured on 1982-019) and failure of a Geosynchronous Orbit Earth Satellite (GOES) 5 encoder lamp.
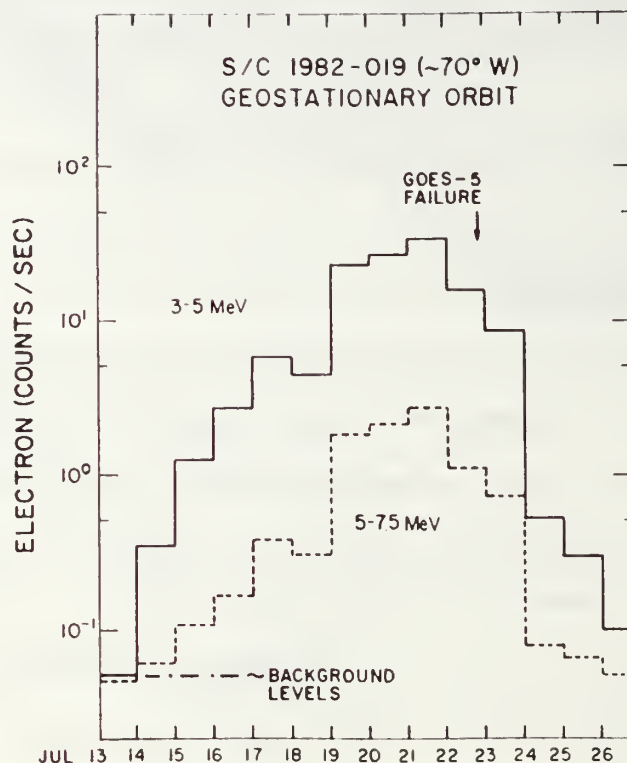

Figure 13

[Ref 6]

Another clear indication of the high energy electron flux-anomaly cause and effect relationship is shown in Figure 14. Over a period of two years, spacecraft 1979-053

22

experienced multiple malfunctions in its star tracker
system, as indicated by arrows above 3 MeV fluxes. Notably,
anomalies occurred only when the electron flux exceeded
approximately 6 count rate units. After several days of
erratic upsets, the anomalous behavior disappeared [Ref 6,
p. 4-1 to 4-16].

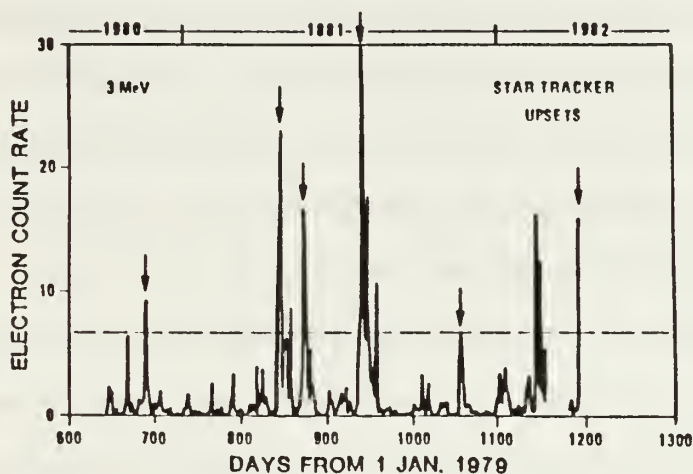

Figure 14

[Ref 6]

D.   Summary

Surface and differential charging are common occurrences
on geosynchronous satellites. Deep dielectric charging can
also occur in the presence of high energy electron fluxes.
These mechanisms are important aspects of spacecraft
operation and survivability. This thesis will build on the
work done in previous examinations of spacecraft charging
and extend it.

III. THEORY OF CHARGING

A. The Environment

Charging is the buildup of charge on the surface and within the body of a spacecraft immersed in a plasma. The plasma environment considered here is the magnetosphere, particularly at geosynchronous orbit. The plasma at geosynchronous orbit has it's origins in the solar wind and the earth's ionosphere. These sources of electrons and ions continually introduce energetic particles into the earth's geosynchronous altitude region where stationary satellites orbit. The energies of the particles vary from fractions of an eV to MeV. Magnetospheric storms and sub-storms inject high energy particles into this region. This is especially common from 2000 LT to 0900 LT, when geosynchronous spacecraft transit the plasmasheet.

The distribution function, or phase space density, characterizes a plasma. Equation (1) shows a Maxwellian distribution, as a function of the velocity of the particles. Such distributions are often used to describe the plasma observed at geosynchronous orbit.

$$(1) \qquad f(v) = n \left(\frac{m}{2 \pi kT} \right)^{3/2} e^{- \left(\frac{mv^2}{2kT} \right)}$$

The temperature, kT, is a measure of the average energy of
the distribution, where k is Boltzmann's constant, and T is
the temperature in Kelvin. Electron volts (eV) are also
commonly used units. The mass of the species is m, the
velocity of the particles is v, and the density n.

Flux, or flow, denoted by J_0, is equal to the product of
the particle charge, density, and velocity. We will need to
relate J to the currents and the particle detector
measurements. The concept of flux can be further defined by
including the originating direction of the particles. Then
the equation $j_0 = J_0/4\pi$ defines a portion of the omni-
directional flux arriving from a particular direction. This
implies that the surface is always perpendicular to the
incident flux. In order to account for the flux from
directions that are not normal to the surface, the equation
must be integrated over all angles from which particles are
incident onto the surface, denoted by d**A**, where d**A** is an
outward vector normal to the surface. The particle
detectors used on spacecraft, typically electrostatic
analyzers, are designed to measure a wide range of energies

by sequentially sampling a specific energy range over a small angle of incidence. Consider one energy channel to be between and energy E and E + dE, along a solid angle, denoted by dΩ, and over a time period from t to t + dt. These parameters will then define the flux of particles within a specified energy range, from a specific direction, at one location, over a distinct time interval incident onto a surface area of the satellite. The measurement in each energy channel gives differential energy flux j [Ref 3, p. 36 to 37]. Figure 15 illustrates the angles associated with differential flux measurements.
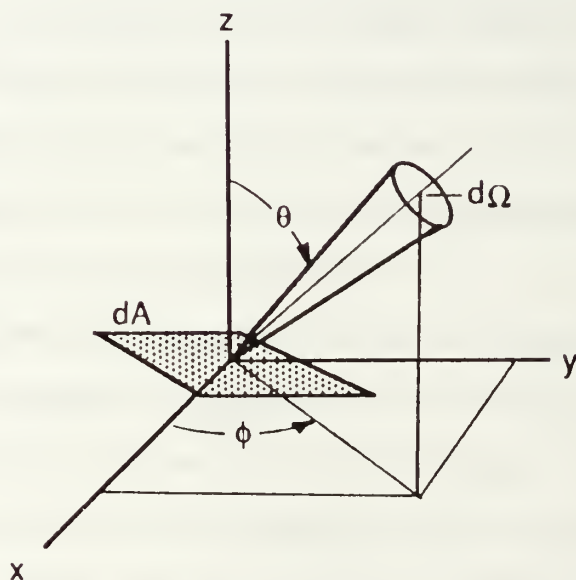

Figure 15

[Ref 3]

Equation (2) expresses the differential flux.

26

$$dN = \vec{j} \cdot d\vec{A} \; dE \; d\Omega dt \qquad (2)$$

The units of differential flux are # / (cm^2 s ster KeV).

To find the distribution function from the differential flux, consider non-relativistic particles in velocity space. The relationship between energy and velocity is given by the equation $v^2 = 2 \cdot E/m$. Using this relationship, the number of particles in a solid angle $d\Omega$ in the energy range dE can be expressed in a velocity space volume by $v^2 \; dv \; d\Omega$. The number of particles in a unit volume of space is then given by the distribution function f multiplied by the number of particles with velocity v in a time t incident on an area dA. Since this is the same as equation (2), the differential flux j is therefore related to the distribution function f by the equation $j = f \cdot v^2/m$ [Ref 3, p. 36 to 38].

This thesis assumes that space is isotropic, that the distribution of particles does not have a preferred direction. By assuming an omni-directional flux, the distribution of particles can be characterized by a single Maxwellian, where particle velocities are independent of orientation. This characterization of the particle distribution gives an accurate description of the plasma at lower energies. When the particle flux has a high energy component out on the tail of the distribution, other mathematical descriptions are used in conjunction with the

27

Maxwellian. The higher energy particles used herein are characterized by an inverse power law.

Further assumptions about the plasma are that it exists in a charge-balanced state. This concept of quasi-neutrality states that the overall charge of the plasma will be neutral. Additionally, the Debye length is large enough for statistical concepts to have meaning. This implies that collisions are rare and particle interaction can be neglected [Ref 3, p. 22].

From kinetic theory, the average energy of a species in an ensemble can be represented by

$$(3) \qquad \overline{E_i} = \overline{\frac{1}{2} m_i v_i^2} = \overline{\frac{3}{2} k T_i}$$

where E_i is the average kinetic energy, v_i is the average velocity, and T_i is the temperature, all of the ith species [Ref 3, p. 27]. This implies that

$$(4) \qquad V_{thermal} = \sqrt{\frac{KT}{m}} \ .$$

From equations (3) and (4), it can be seen that in an equi-temperature species, the electron velocity is at least 43 times the ion velocity, by virtue of their light mass.

Therefore, for comparable temperature, the effects of ions can largely be ignored.

B. Surface Charging

Spacecraft are constructed from conducting and insulating materials. Metal surfaces provide a ready pathway for incident charges to re-distribute themselves. Insulators or dielectrics, on the other hand, do not easily allow charges to move within or over them. As particles of varying energy hit the satellite surfaces, some strike conductors and move to establish equi-potential surfaces. Other particles collide with dielectrics and are fixed, thus establishing electric fields over localized portions of the spacecraft surface. These electric fields are dynamic in nature, always trying to move the charge to positions of minimum energy.

The distribution of charge and currents on the spacecraft surface at equilibrium will minimize the potential energy. This implies that any charge on the satellite surface will, if mobile, arrange itself, with respect to the plasma currents and surface potential, at minimum energy.

The balance of currents entering and leaving the surface of a satellite can be characterized by equation (5)

$$(5) \qquad \vec{J}_{net} = \vec{J}_{ambient} + \vec{J}_{energetic} + \vec{J}_{secondary} + \vec{J}_{backscatter} + \vec{J}_{hv}.$$

True ambient flux is all of the flux that surrounds the spacecraft. Ambient current density is current/unit area that comes from the ambient flux.

A distinction is made here regarding the ambient and energetic fluxes. Even though both come from the overall ambient flux, there is an artificial break point established at 40 keV. At this point, the description of the distribution function changes from a Maxwellian to an inverse power law. Therefore, it is easy to separate the two current densities in a similar way.

The secondary current density comes from incident electrons that knock lose one or more electrons from the material surface. Electrons that are reflected from the surface are included in the backscatter term. Finally, the photoelectric term accounts for electron emission of bound electrons from the surface (photon energy > material work function).

Figure 16 shows how each of the current densities in

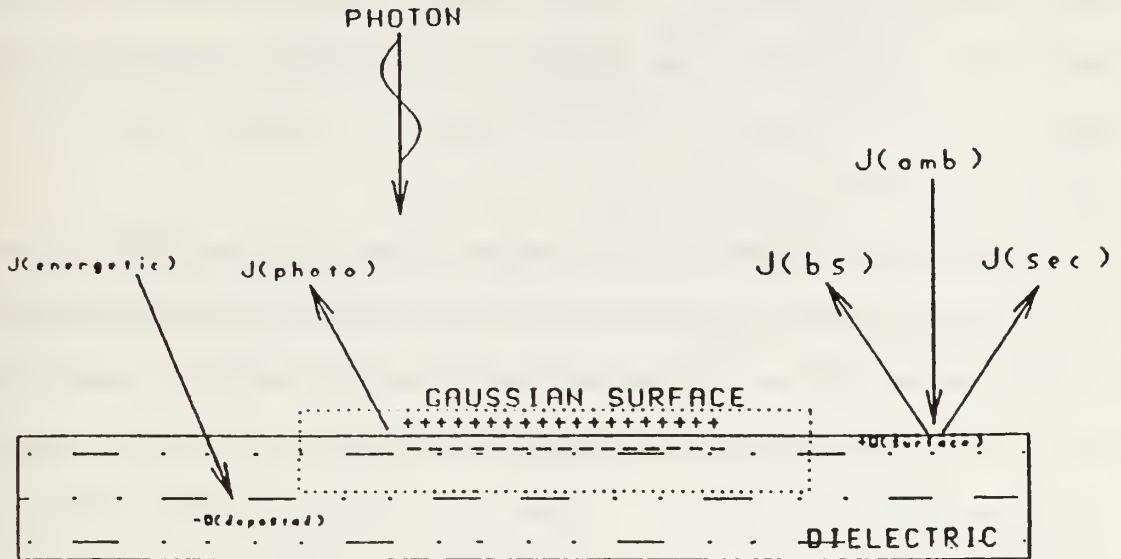equation (5) contributes to the net current density at the spacecraft surface.

Figure 16

[Ref 23]

Equation (6) shows that the current density is proportional to both the electron density and the temperature.

$$(6) \qquad\qquad \vec{J} = q\, n\, \vec{V}_{thermal}$$

where q is the charge of the species, n is the density, in particles / volume, and $V_{thermal}$ is given in equation (4).

The net current density is dependent on many different parameters. The temperature of the ambient and energetic distributions, plasma density, velocity of the spacecraft in the plasma, percentage of projected area that is dielectric, materials from which the dielectric surfaces are made, and whether the satellite is in sunlight or eclipse, are all factors in determining J_{net}.

Additional sources of current come from secondary ion emission, movement of the satellite across local magnetic fields or relative to the ambient ion population, ions from satellite outgassing, and induced current flows from high differential potentials. These are usually minor effects that will be ignored. [Ref 1, p. 2-1, Ref 24, p. 168]

Equation (5) describes a delicate balance between different mechanisms that contribute to the surface charge of a spacecraft. In turn, each of the contributions to J_{net} will be examined.

1. **Ambient Current Density**

Current density equals the charge multiplied by the flux. The flux is found when differential energy flux is integrated over the applicable energy range. The flux is given by

$$(7) \qquad \Phi = \iiint f(\vec{v}) \cdot (\vec{v} \cdot \hat{n}) \, d^3\vec{v}$$

where the f(v) is given by

$$(1) \qquad f(\vec{v}) \;=\; n \left(\frac{m}{2\pi kT} \right)^{3/2} e^{-\left(\frac{mv^2}{2kT} \right)} .$$

The particles incident on the surface area from non-normal angles is accounted for in the (v · n) term in equation (7) [Ref 22]. Using spherical coordinates, the flux in velocity space can be expressed as

$$(8) \qquad \Phi \;=\; n \left(\frac{m}{2\pi kT} \right)^{3/2} \int_{v_{min}}^{v_{max}} \int_{0}^{\pi/2} \int_{0}^{2\pi} e^{-\left(\frac{m v^2}{2 kT} \right)} v^3 \cos\theta \, \sin\theta \, d\phi \, d\theta \, dv.$$

The angular integration gives a factor of π. By using the relationship $E = \frac{1}{2}mv^2$, the integration can be done over the distribution function energy range. This gives

$$(9) \qquad \Phi \;=\; n \left(\frac{kT}{2\pi m} \right)^{1/2} \int_{E_{min}}^{E_{max}} e^{-\left(\frac{E}{kT} \right)} E \, dE .$$

The flux is the integral of the differential energy flux, J(E), integrated over the energy range. The differential energy flux is

33

$$(10) \qquad J(E) = n \left(\frac{kT}{2\pi m} \right)^{1/2} e^{-\left(\frac{E}{kT} \right)} E .$$

2.   Secondary Emission Current Density

Electrons incident on a spacecraft surface can undergo anyone of three interactions, reflection, backscattering, and secondary emission. Reflection of electrons is a extremely low energy phenomena, generally found at energies below 10 eV, and can be neglected [Ref 23].

When low energy electrons collide with the satellite surface, they quickly come to rest. The energy from the incident electrons becomes available and may be absorbed by bound electrons. If this energy is sufficiently high, one or more electrons may be ejected from the surface material.

Secondary electrons will be ejected at a low energy, generally with an energy below 50 eV. More than 80% of all secondary electrons have energies below 20 ev [Ref 30, p. 163 to 189]. A secondary yield term, attributed to Sternglass (1950), is material and ambient flux dependent.

$$(11) \quad Yield_{secondary} = 7.4 \cdot \delta_{max} \left(\frac{E}{E_{max}} \right) e^{-2 \left(\frac{E}{E_{max}} \right)^{1/2}}$$

34

where E_{max} is the energy where yield$_{secondary}$ is the greatest and δ_{max} is the secondary yield at E_{max}. Table 2 shows secondary emission properties for various spacecraft materials [Ref 23, p. 41, Ref 25, p. 123, Ref 26, 493 to 499, Ref 27].

TABLE 2

MATERIAL	E(max) eV	δ(max)
Gold	800	1.45
Oxidized Aluminum	300	2.60
Silicon Dioxide	420	2.50
Aquadag	350	0.75
Teflon	200	3.00
Kapton	250	1.80

Figure 17 shows a graph of the secondary electron yield for kapton as a function of the incident electron energy.

The figure is typical for most spacecraft materials. The maximum yield on the curve, usually from an incident electron at a few hundred eV, results in more than one electron ejected from the surface.

In the figure, secondary emission electrons outnumber incident electrons between 50 eV and 1 keV. These two energies, where the secondary yield is one, are known as the lower and upper crossover energies, respectively. If the ambient flux is sufficiently rich in particles between the two crossover energies, more electrons will leave the surface than are deposited, $J_{secondary} > J_{ambient}$, and the spacecraft will charge positively, typically a few volts positive.

The upper crossover energy suggests the threshold energy effect. When the electron distribution function contains sufficient high energy components and of sufficient energy to balance the out-flux of secondary electrons, the satellite potential will become negative. Therefore, the temperature of the ambient electron distribution will be instrumental in the determination of the spacecraft potential. The energy at which balancing occurs is known as the threshold energy and is the start of negative charging.

The threshold energy will vary among spacecraft because of geometry and dielectric materials, but lies

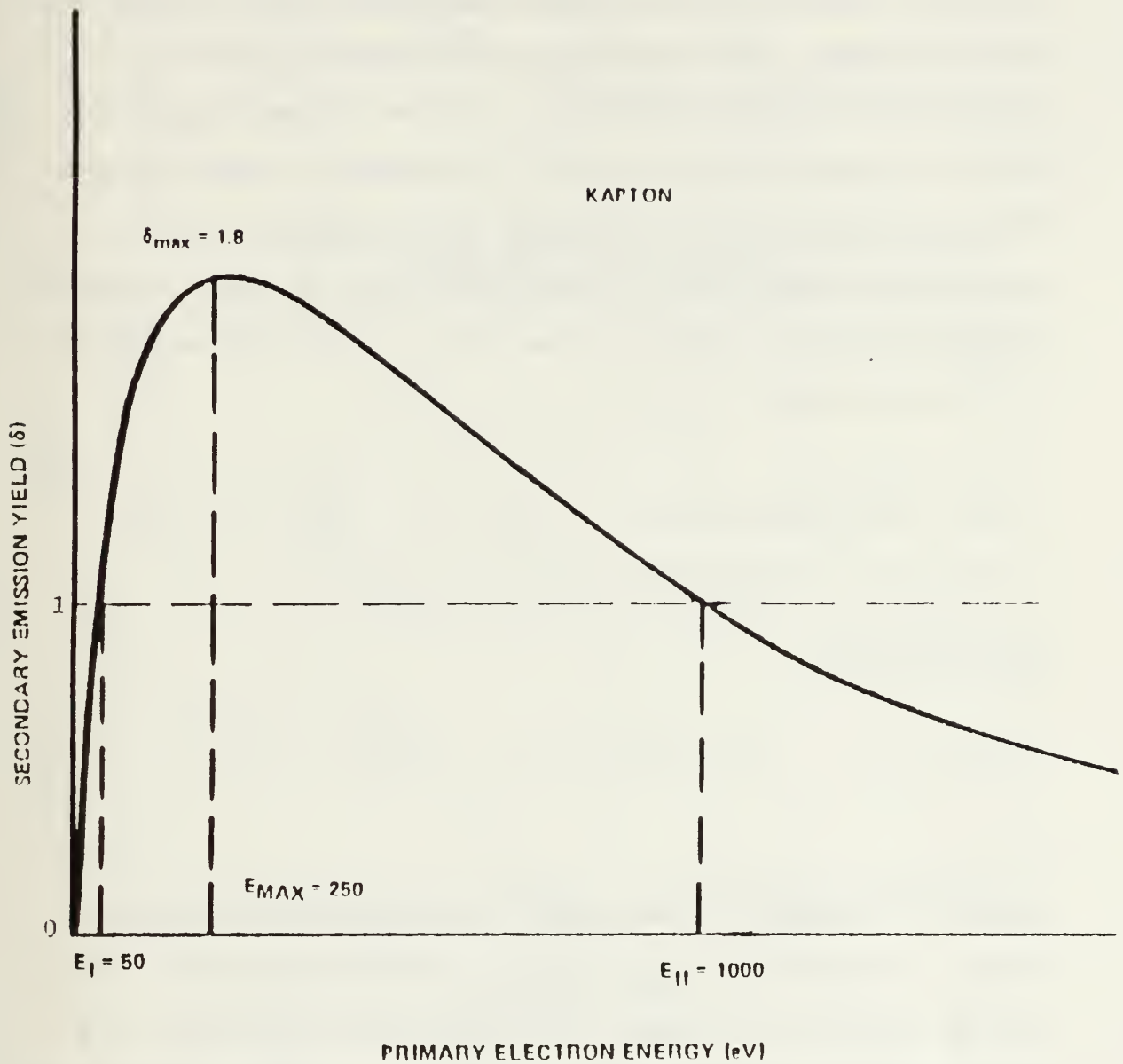within the 10 to 20 keV band [Ref 26, p. 493 to 499, Ref 39, p. 169 to 175].

Figure 17

[Ref 26]

3. Backscattered Current Density

The ambient flux electrons have different kinetic energies. As electrons hit the satellite surface, some reflect, others cause secondary emission, still others are backscattered. Backscattering is primarily elastic collisions (coulomb scattering) of the incident particles with the surface atomic nuclei. Low-energy electrons are deflected into a wide scattering cross-section. The responsible mechanism is complicated, but a useful model for backscattered electrons is [Ref 25, p. 104 to 105, Ref 29, p. 1969 to 1981]

$$(12) \quad Yield_{backscattered} = 0.1 \left(1.0 - \frac{.05}{E}\right) \left(\beta + e^{-\frac{E}{5.0}}\right)$$

β is given by

$$(13) \qquad \beta = 10.0 \left(1.0 - \left(\frac{2.0}{e}\right)^{(0.037 \cdot Z)}\right) .$$

where E is energy in keV and Z is the effective atomic number. This formula is good for incident electrons with energy $\geq$ 50 eV. Incident electrons with less energy are counted along with secondary emissions. Figure 18 shows how the backscatter emission curve determines the backscatter flux for a Maxwellian distribution with T = 7.7 keV and n = 0.15 cm^{-3}.
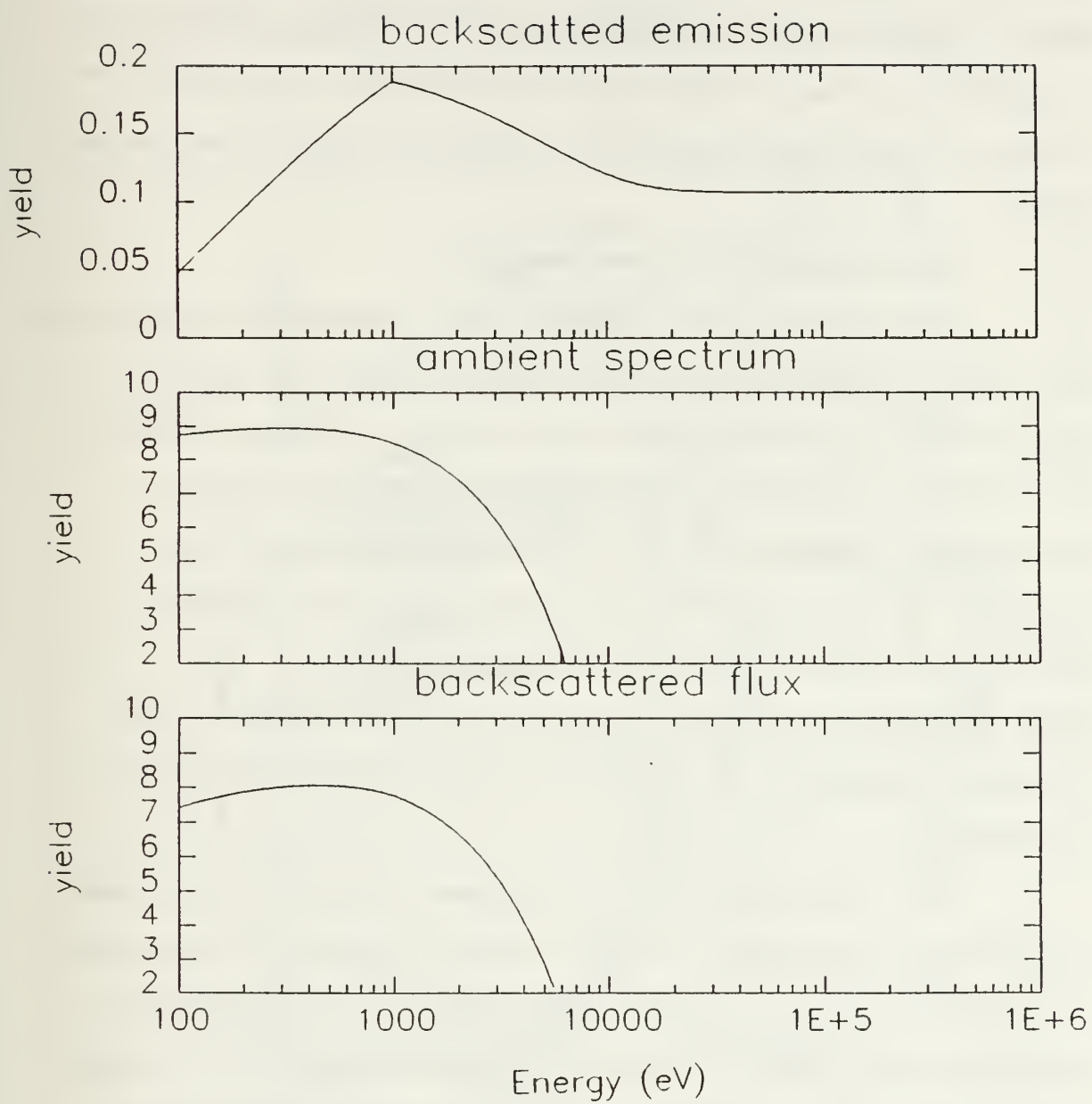
Figure 18

39

Two transcription errors were noted in References 23 and 25. The exponential term in β was not raised to a power, and the 0.05 was written as 0.5. This could have resulted in a very slight under-calculation of the backscattered flux between 100 and 500 eV in the referenced work.

4. Photoelectric Current Density

When photons are incident on a spacecraft, electrons are ejected from the surface, provided that the energy of the photons is greater than the electron binding energy of the surface molecules. Typically, the photon energy spectrum is higher than the threshold energy or work function of the material. The photoemission electrons, therefore, have an energy spectrum (1 to 15 eV) that modulates with the photon spectrum, but is lower by the threshold energy. Saturation current densities range up to 42 $\mu A/m^{-2}$.

The wavelength of the incident photons is inversely proportional to their energy. Figure 19 shows a comparison of the solar flux to photon wavelength, and the resultant photoemission yield. A λ of 10^4 Å corresponds to a photon energy of 1.2 eV, $3 \cdot 10^3$ Å to 4.1 eV, and 10^3 Å to 12.4 eV. For tungsten, incident photons ≥ 10 eV eject an electron 1% ~ 25% of the time [Ref 31].

40

Table 3 lists saturation current densities for spacecraft materials, mean kinetic energy upon ejection from the surface, and the electron density next to the ejecting surface.
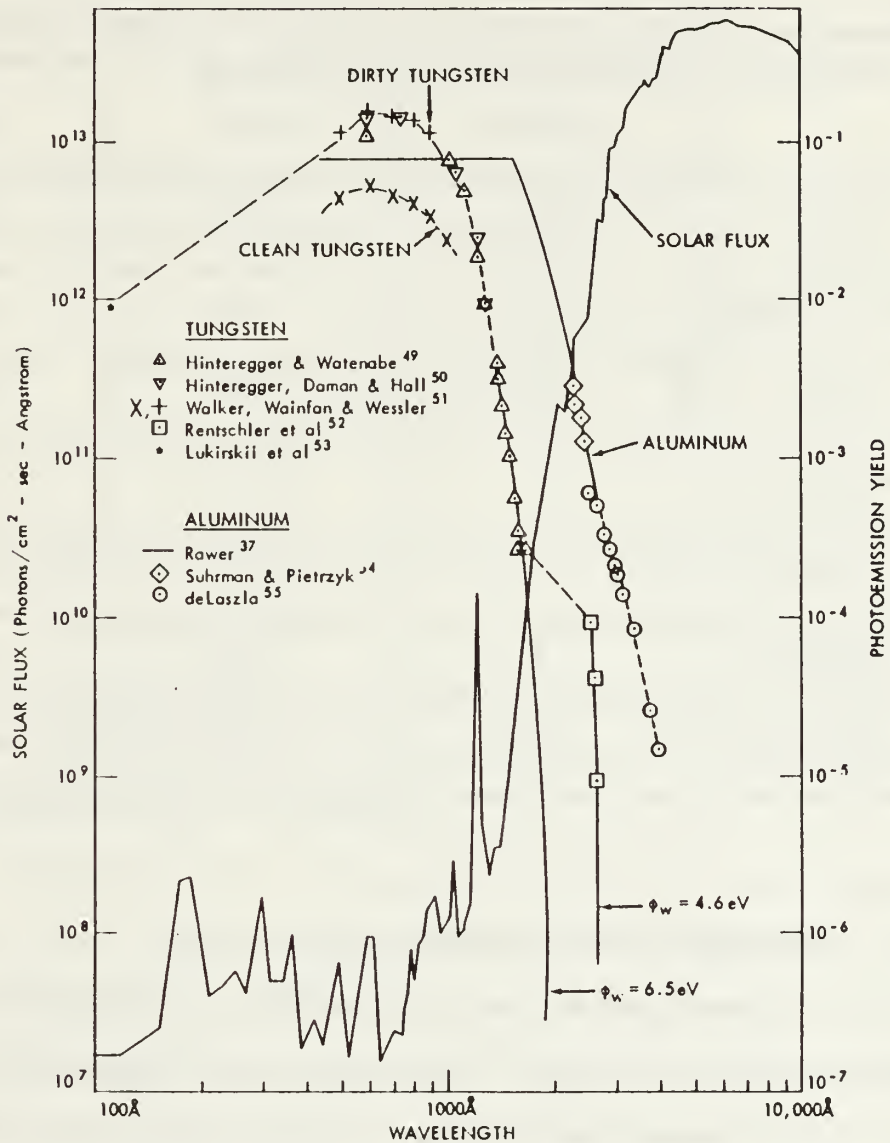

Figure 19

[Ref 30]

41

Table 3 summarizes computed photoemission values for typical
spacecraft materials [Ref 30, p. 163 to 189].

TABLE 3

Material	Saturation J $(\mu A/m^2)$	$<E_{kinetic}>$ (eV)	e⁻ density$_{surf}$ (cm^{-3})
Al_2O_3	42	1.33	1670
Indium Oxide	30	1.35	1260
Gold	29	1.40	1110
Aquadag	18	1.17	500
Cr. Steel	20	1.42	770
Graphite	4	1.48	150
Average	21	1.42	830

5. Energetic Current Density

The energetic current density is that portion of the
electron spectrum which is no longer well-described as a
Maxwell-Boltzmann distribution. We use the term energetic
here to signify that the differential flux component comes
from a power law distribution, which begins at approximately

42

40 keV for data considered here. The distribution function
is proportional to $(E/E_0)^{-x}$, where x typically 4 to 6. In
our case, x = 5 (this gives a flux that in proportional to
E^{-3}). The flux is found when differential energy flux is
integrated over the applicable energy range.

$$(7) \qquad \Phi = \iiint f(\vec{v}) \cdot (\vec{v} \cdot \hat{n}) \; d^3\vec{v} .$$

Now f(v) is given in terms of energy by

$$(14) \qquad f(E) = n \; \frac{7}{4\sqrt{2}\pi} \left(\frac{m}{q \, E_0} \right)^{3/2} \left(\frac{E_0}{E} \right)^5$$

The distribution function is given in terms of energy. The
mass is m, q is the charge, E_0 is the minimum energy for the
distribution function, in eV [Ref 13, p. 5568 to 5578, Ref
22]. The normalization is such that n = $\iiint$ f(E) when done   '
with limits E = E_0 to infinity.

Inserting the distribution function into equation 7,
and using the relationship E = ½mv², the integration can be
done over the distribution function energy range. The upper
limit of integration is infinity. Since the distribution
function tail asymptotically approaches zero, the
contribution from the upper limit is zero. Therefore, the
energetic flux is primarily determined by the lower limit of
integration.

Inserting equation (16) into (7) gives

$$(15) \qquad \Phi = n \; \frac{7}{2\sqrt{2}} \; \sqrt{\frac{E_0 q}{m}} \int_{E_{min}}^{\infty} \left(\frac{E_0}{E} \right)^4 \frac{dE}{E_0}$$

As with the ambient differential energy flux (equation 11), the energetic differential energy flux is given by

$$(16) \qquad J(E) = n \; \frac{7}{2\sqrt{2}} \; \sqrt{\frac{q}{mE_0}} \left(\frac{E_0}{E} \right)^4 .$$

To summarize, the positive contributions to the net current density (positive is defined as into the satellite surface) are the ambient flux, which is the Maxwellian flux from 0 to 40 keV, and the energetic flux, which accounts for the energetic electrons above 40 keV. Countering the positive flux are the secondary, backscatter, and the photoelectric current densities.

Table 4 gives an order of magnitude comparison of which current densities are important and which mechanisms can be ignored.

TABLE 4

CURRENT DENSITY SOURCE	FLUX (e/m²s)	J (μA/m²)
Ambient (Φ < 40 keV)	3.0×10^{12}	.48
Energetic (Φ > 40 keV)	1.4×10^{11}	.02
Backscatter	3.2×10^{11}	.05
Secondary	1.6×10^{12}	.26
Photoemission	1.3×10^{14}	21.

The largest contributor to the net current density is the photoelectric term, by approximately two orders of magnitude. When the spacecraft is in eclipse, however, the ambient flux provides a net accumulation of electrons to the surface, and the vehicle would charge negatively. This is closely followed by the secondary emission current density.

45

The distribution function used here is for a hot plasma distribution, where the temperature is higher than for a quiet day. During quiet days, when the ambient and energetic fluxes would be lower, the sum of the secondary and backscatter terms would be closer to the positive fluxes. This would allow the net current density to self-balance, precluding large negative potentials from forming.

The effect on the potential from the net flow of charge to the surface of the spacecraft is clearly shown in Figure 20. On 20 September, 1974, ATS 5 and ATS 6 were immersed in the same plasma, and both charged to similar negative potentials, prior to the active experiments which were the focus of this work. An experiment on spacecraft potential modification was conducted with the electron source on ATS 5. The electrons came from a filament source, from ~ 0632 to 0635 [Ref 38, p. 527 to 532]. Prior to 0632 and after 0635, ATS 5 and ATS 6 charged to the same potential.

This shows that although surface material characteristics are important (e.g., secondary yield), variations between these vastly different vehicles did not lead to greatly different potentials in eclipse. Hence, simple assumptions about yield terms, such as assigning "typical" values for glass or aluminum are not unreasonable.
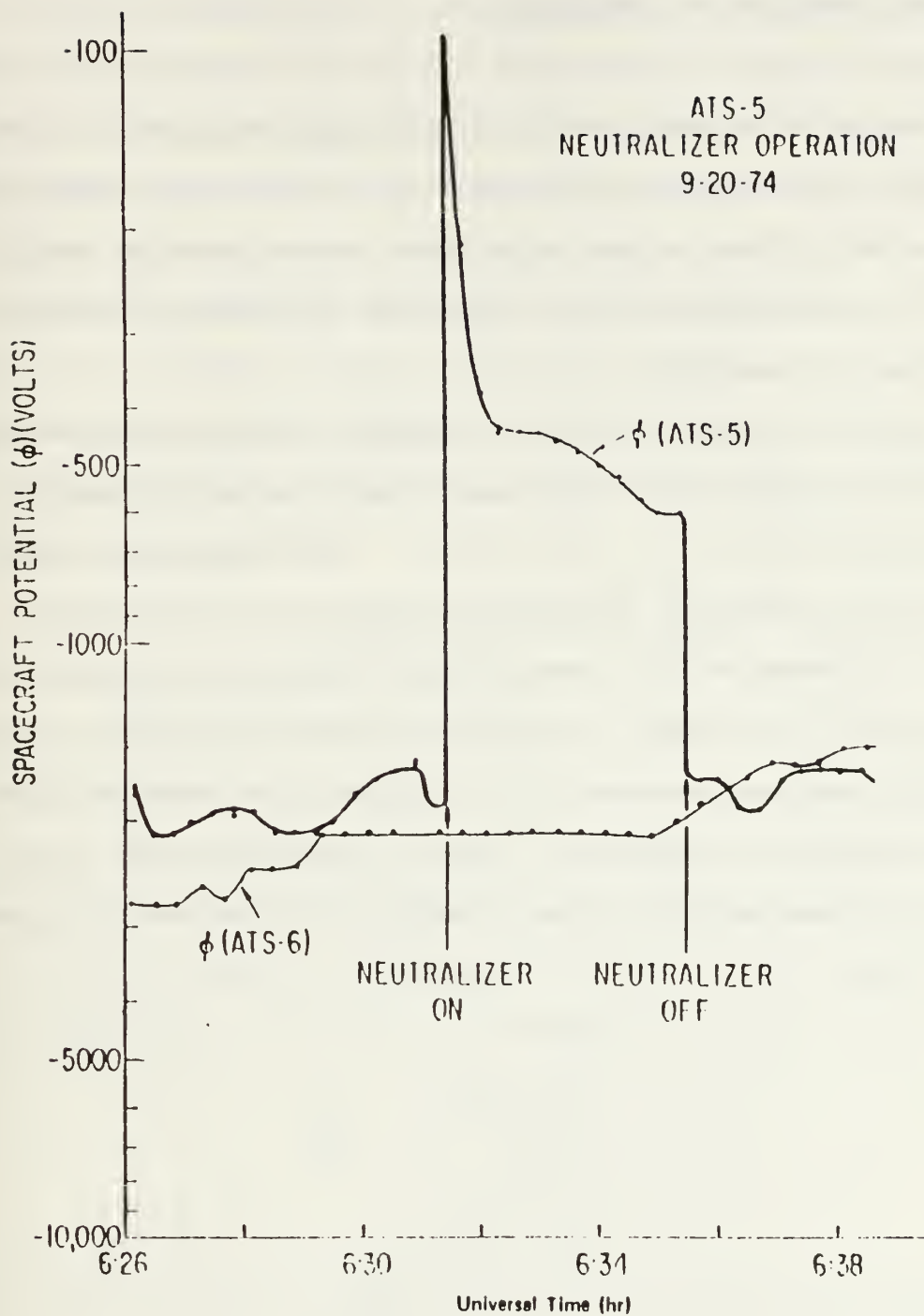
46

Figure 20

[Ref 38]

47

C. Deep Dielectric Charging

Energetic electrons lie in the high-energy tail of the electron distribution function. As the average temperature of the distribution increases, the number of high energy particles increases, and so does the likelihood of deep dielectric charging.

In 1976, a new charging mechanism was proposed in which high energy electrons imbedded themselves in dielectric materials [Ref 36, p. 237 to 246]. This mechanism, deep dielectric charging, becomes important when the ambient electron distribution function has a high-amplitude high-energy tail. Through secondary and photoemission, or solely through secondary emission in eclipse, the surface layer can become electron depleted. This, in turn, creates large electric fields within the dielectrics as shown in Figure 21.
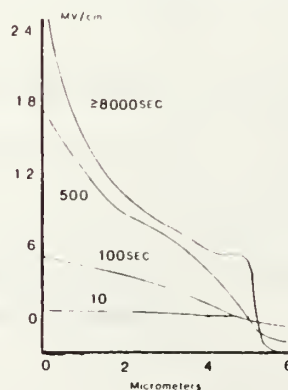

Figure 21

[Ref 37]

48

When the top layer is "hole" rich, the electric fields that are produced are on the order of 10^6 volts per cm. As time increases from minutes to hours, the potential will draw electrons within the dielectric toward the surface.

The consequence of "energetic electrons" in the distribution function is deep dielectric charging. Important results of deep dielectric charging are energy deposition profiles, radiation-induced conductivity, localized formation of strong electric fields, and formation of potential barriers.

The build up of charge within the dielectrics is governed by two competing processes, the rate which charge is deposited, and the rate which it leaks out. The net charging rate can be modelled by considering the dielectric to be a one-dimensional slab of thickness d. If the current density entering is J_i and J_o is that which exits the dielectric, then the divergence of the current density is approximately $(J_i - J_o)/d$. The continuity equation

(17)
$$-\frac{\partial \rho}{\partial t} = \vec{\nabla} \cdot \vec{J}_D + \vec{\nabla} \cdot \sigma \vec{E}$$

can then be used to model the net rate of accumulation. Equation (18) shows the mechanism for the net buildup of charge, but does not include surface conductivity effects, as modified by radiation.

Solving the continuity equation for charge density as a function of time , assuming no charge at t = 0, as would be the case when the spacecraft environment is calm and there is photoemission, gives

$$(18) \quad \rho(t) = \frac{J_i - J_o}{d} \frac{\varepsilon}{\sigma} [1 - e^{-\frac{\sigma}{\varepsilon}t}]$$

These simple equations show that the time constant $\tau = \varepsilon/\sigma$. For glass, τ is many hours since deposited electrons will remain practically forever.

1. **Radiation-induced Conductivity**

The conductivity in equation (18) is a free parameter in the charge balance equation. The conductivity of the dielectric can be altered over time by a phenomena known as radiation-induced conductivity (RIC). This effect varies with the depth of the material, and is confined primarily to the surface of the dielectric. The effects of RIC will be discussed below. First the electron deposition process must be considered.

2. **Energy Deposition Profile**

The energy deposition process is a complex mixture of elastic and inelastic collisions, scattering, and material penetration, as described by scattering theory [Ref 32, p. 2-1, 2-2]. Figure 22 shows the deposition depth of electrons in silicon glass as a function of the incident

50

particle energy [Ref 35, p. 123].   The significance is that
for a 12 mil (0.03 cm) cover cell, electrons from several
hundred eV to approximately 225 keV will deposit themselves
within the dielectric.   Electrons with higher energies will
pass through and enter the spacecraft body.   At the low
energy limit (10 keV) electrons reach approximately 1.5 x
10^{-4} cm, or 1.5 μ into the material.   We take this as being
the minimum energy limit for charge deposition.   Electrons
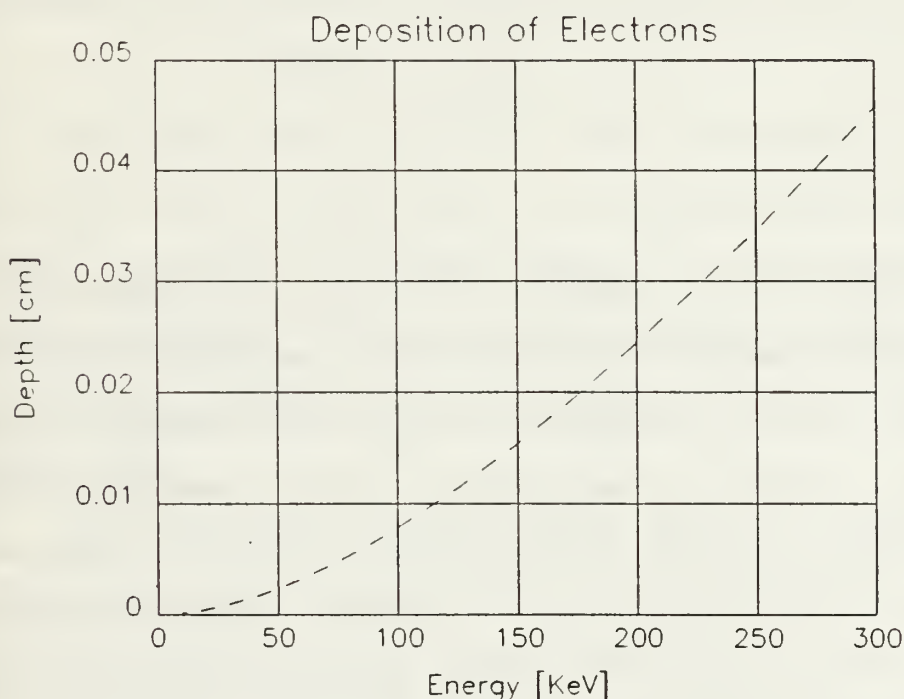deposited at lesser depths will flow rapidly along the
surface.

Figure 22

[Ref 35]

51

The effective conductivity of the dielectric is a combination of the intrinsic conductivity σ_i and the radiation-induced conductivity σ_{RIC}, and can be expressed as

$$(19) \qquad \sigma_{effective} = \sigma_i + \sigma_{RIC}$$

[Ref 33, p. 2282]. Radiation-induced conductivity can be modelled by

$$(20) \qquad \sigma_{RIC} = K \, \dot{D}^{\Delta}$$

where K is the coefficient of RIC, and Δ is a material dependent parameter. Although theory predicts that both are constants and are independent of type and energy of the radiation, there is disagreement on their empirical values. Δ is frequently found to lie within 0.9 to 1.1, and can be taken as 1.0. K lies within a greater range of minimum and maximum values, hence introduces greater uncertainty into equation (20) than does Δ.

Table 5 lists maximum and minimum values for typical
spacecraft dielectrics. Units are 10^{-19} sec/(Ω cm rad) [Ref
34, p. 580].

TABLE 5

Material	K_{max}	K_{min}
Kapton	60	1.2
Teflon	1000	20
Mylar	2.1	1.8

The dose rate in equation (20) is given by dD/dt,
and is the rate at which energy is deposited into the
material, in units of rads per second. A rad is defined as
100 ergs per gram. The dose rate consists of three parts,
the collision stopping power, the specific thickness, and
incident flux.

The collision stopping power (CSP) is a measure of
how far into a material electrons will penetrate as a
function of their incident energy and the thickness of the
material. By dividing the CSP by the density of the
material, the CSP becomes independent of the material and
comparative analysis can be performed. At low energies, the
CSP measure loses its usefulness, and ceases to be

meaningful at energies below several hundred eV [Ref 35, p. 20]. The units of CSP are MeV-cm^2 / gm. Figure 23 shows CSP as a function of the energy for borosilicate, "pyrex" corning 7740 glass, density = 2.23 gm/cm^3. This is similar to the material used for solar array cover cells.
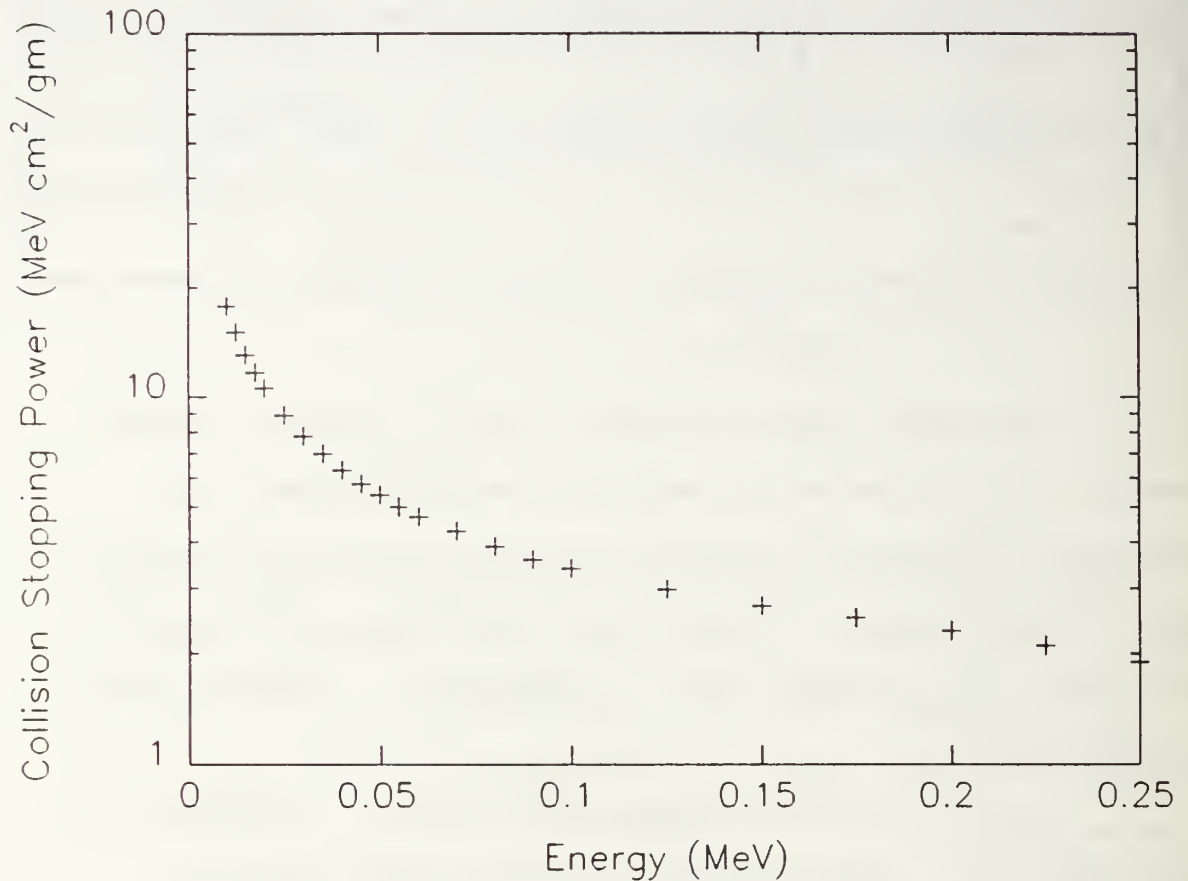

Figure 23

[Ref 35]

The dose profile in a low atomic number (low-Z) material is directly proportional to incident kinetic

54

energy. By defining the incident thickness in terms of e^-
/cm^2-MeV, the dose profile will be independent of the
particle's incident energy and the nature of the material.
This thickness is defined as specific thickness (T_s), and is
given by

$$(21) \qquad T_s = \frac{\rho \; x \; N_0}{T} \sum_i f_i \left(\frac{Z}{A}\right)_i$$

where f_i is the weight fraction of the ith element of the
material, and is given by

$$(22) \qquad f_i = \frac{n_i \; A_i}{\sum n_i \; A_i}$$

and where the parameters are defined as:

- ρ = material density (gm/cm^3)
- x = depth in the material in cm
- N_0 = Avogadro number
- T = e^- energy in MeV
- A = Atomic weight
- n_i = number of atoms in the ith element of the material

The incident differential energy flux is calculated from the
plasma parameters in units of $e^-/(cm^2$ s ster MeV).

55

The front surface dose is found by multiplying the differential energy flux with the CSP. The dose profile in a low Z material is calculated by finding the front surface dose and then modulating it with the curve in Figure 24. The dose rate is then calculated by integrating the dose profile over the applicable energy range.

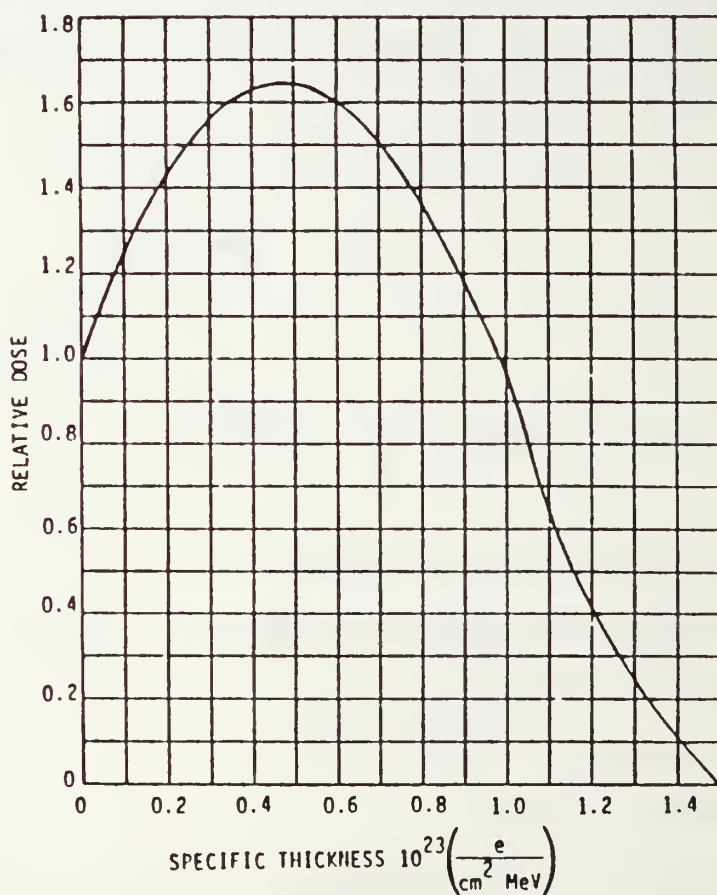Figure 24 plots the incoming flux, or relative dose, against specific thickness (T_s).

Figure 24

[Ref 32]

56

If the saturation electric field at any time exceeds the dielectric breakdown threshold, as modified by RIC, charge re-distribution or arcing will occur.

Using a teflon sample (d = 10 mils), a breakdown threshold of 10^7 coulombs/cm^2 and a discharge time of roughly 50 nanoseconds, peak structural currents (geometry dependent) can range from 1 to 10 amps [Ref 33, p. 2281 to 2284]. The use of teflon, a dielectric material, is for an order of magnitude picture of the peak currents that can occur.

D. Potential

The overall charge of the spacecraft determines the potential. The charge density on the spacecraft is determined by the net current density, as shown in equation (5), integrated over the appropriate time interval. We tacitly assume the currents are constant over the periods of integration.

$$(5) \qquad \vec{J}_{net} = \vec{J}_{ambient} + \vec{J}_{energetic} + \vec{J}_{secondary} + \vec{J}_{backscatter} + \vec{J}_{h\nu}$$

For the two different charging mechanisms identified, surface and deep dielectric charging, the appropriate time constants are very different.

57

For surface charging, the time periods which are appropriate are typically a second or less. This is because the relatively small capacitance associated with satellite potentials can lead to significant charge buildup (changes in potential) within a millisecond time frame. If the satellite is near equilibrium, the net current will be small, and it should be possible to estimate the net charge density accumulated in one spin period by taking the currents to be constant over that period.

$$(23) \quad q/m^2_{surf} = (J_{amb} - J_{photo}/2 - J_{sec} - J_{bs}) \cdot spin\ time$$

Sunlight shines on approximately 20% to 25% of the spacecraft surface at any given time, depending on the vehicle geometry. The spin time for a satellite can range from less than a second to about one minute per revolution.

In deep dielectric charging, the charge density comes from the energetic current density. Therefore, the deposition of charge is dependent on the energetic tail of the distribution function. This gives a net deposition of charge into the dielectric material over long periods of time, that is minutes to hours.

The deposition of charge into the dielectrics will occur slowly, but can eventually become significant if the resistivity is high. Hence the charge distribution can be

58

similar to that induced with shadowed differentially charged surfaces [Ref 40, p. 6809 to 6819].

A potential barrier around the spacecraft can form and grow large enough to suppress low-energy secondary and photoemission electrons. These electrons are returned to the spacecraft and help maintain a negative potential, even in the presence of sunlight. This is the process generally invoked for daylight negative potentials for satellites with insulating surfaces [Ref 28]. This development of differential potentials, or the buildup of trapped charge is a slow process, usually on the order of five to ten, or more, minutes [Ref 8, p. 5657 to 5667]. It is possible that deep dielectric charging could also lead to barriers, and also provide a mechanism for daylight charging [Ref 23]. This is what we want to study further.

If we take the potential of a spacecraft to initially be zero, then in one spin of the vehicle the surface charge density, σ_{photo}, develops from incident sunlight. Can enough charge be trapped so that

$$(24) \qquad \sigma_{deposited} = \int_{one\ hour} J_{energetic}\ d\tau \geq \sigma_{photo} \quad ?$$

If so, we can imagine that a surface starting at $\phi \approx 0$ will at some point develop a net charge which can not be balanced by photoemission in one spin period.

E. Summary

Lower energy ambient flux is responsible for surface charging. This phenomena occurs in eclipse, when the photoelectric emission is blocked. Surface charging appears in a very short time span ($\tau < 1$ second), charges uniformly to several keV, and returns rapidly to equilibrium potential when photoemission is restored.

A second mechanism, deep dielectric charging, occurs when there is an energetic tail on the distribution function. These energetic electrons bury themselves into the dielectrics covering the satellite surface. Movement of the electrons out of the dielectrics is slow (τ can range from seconds to several minutes). If a buildup of charge exceeds the breakdown strength of the material, electrical discharges may cause anomalies in satellite systems.

Associated with deep dielectric charging is the formation of potential barriers. Upon entering sunlight, photoelectrons emitted from the satellite surface are not energetic enough to overcome the potential barrier, and are returned to the satellite, thus maintaining the negative charge. Negative potentials in the range of several hundred volts will remain until the charge buried within the dielectric can leak out.

IV. RESULTS

A. ISEE 1-Observed Integral Flux

1. Ambient Differential Energy Flux

On 17 March, 1978 (day 76), ISEE 1 transited geosynchronous altitude during a period when high energy electrons fluxes were observed. ISEE 1 moved through the plasmasheet and was observed to charge to at least -70 volts in sunlight. The time of maximum charging, near -100 volts, was at 0300 LT. Another geosynchronous satellite, ATS 5, was orbiting through the same plasma environment at local midnight, and charged to -6 kV in eclipse. The indication of charging on ATS 5, indicates that the plasma environment was sufficiently hot for spacecraft charging [Ref 13, p. 5568 to 5578]. Recall that ATS 5 and ATS 6 are two vastly different satellites, but charged to similar potentials in eclipse (Figure 20).

Instrumentation on-board ISEE 1 included two electron detectors, the University of Iowa LEPEDEA, and the Medium Energy Particle Instrument, or MEPI. The LEPEDEA detector data was taken from the radial direction, a 6°x 38°solid angle. The telemetry for this data covered the 200 eV to 45 KeV energy range in 32 steps [Frank et al., 1978].

61

The MEPI covered the 20 to 1200 KeV energy range with eight channels. The detectors provided an angular resolution of 10°x 45° with a geometric factor of 10^{-2} cm^2 ster [Williams et al., 1978].

Figure 25 shows the distribution function recorded by ISEE 1 on day 76. There are three distinct segments to the distribution function that were observed. The low energy segment of electron distribution function was measured from a few hundred eV to one keV. The average temperature was 314 eV and the plasma density was 0.25 cm^{-3}. Figure 25 shows the electron distribution function.
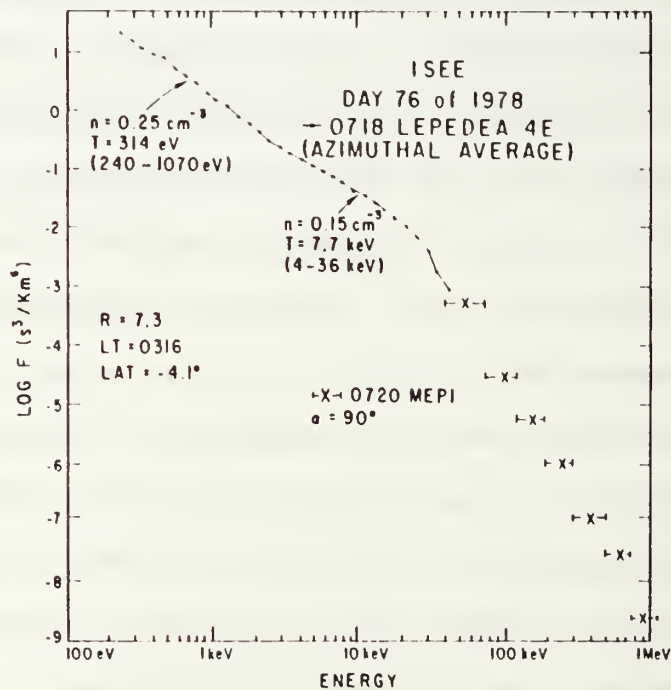

Figure 25

[Ref 13]

62

The second electron population can also be described
as a Maxwellian distribution. The average temperature of
this group of electrons is 7.7 keV and the density is 0.15
cm^{-3}. The data was collected over an energy range of 4 to
36 keV. There is a boundary between the two Maxwellian
distribution functions at 1.7 keV. The values recorded for
the energy spectrum below 40 keV are typical of the plasma
found in the plasmasheet. This data is plotted as a series
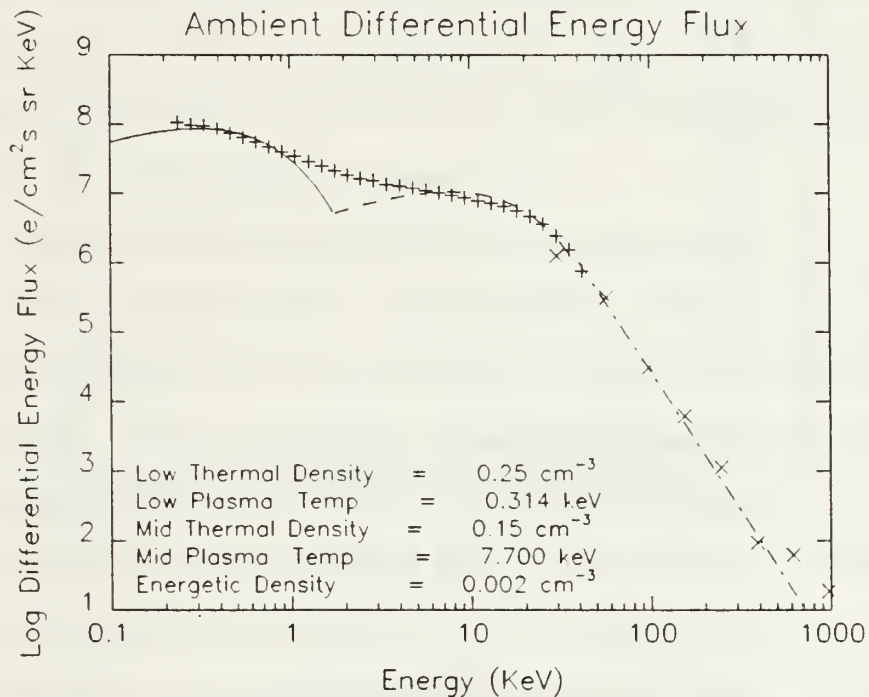of "+", and labelled "low" and "mid" in Figure 26.

Figure 26

Above 40 keV, the MEPI data is plotted with "X", and
is labelled "energetic". The energy spectrum follows an
inverse power law distribution and is approximately

proportional to an E^{-4} distribution function. To smoothly

connect the mid-Maxwellian and the energetic distribution

functions, an energetic density of 0.002 cm^{-3} was fitted.

This fit agrees with the previous work done [Ref 23].

2. **Secondary Electron Differential Energy Flux**

The secondary electron flux produced by this

distribution function is shown as a function of incident

energy in Figure 27.

Secondary Electron Differential Energy Flux

Low Thermal Density = 0.25 cm^{-3}
Low Plasma Temp = 0.314 keV

Energy (KeV)

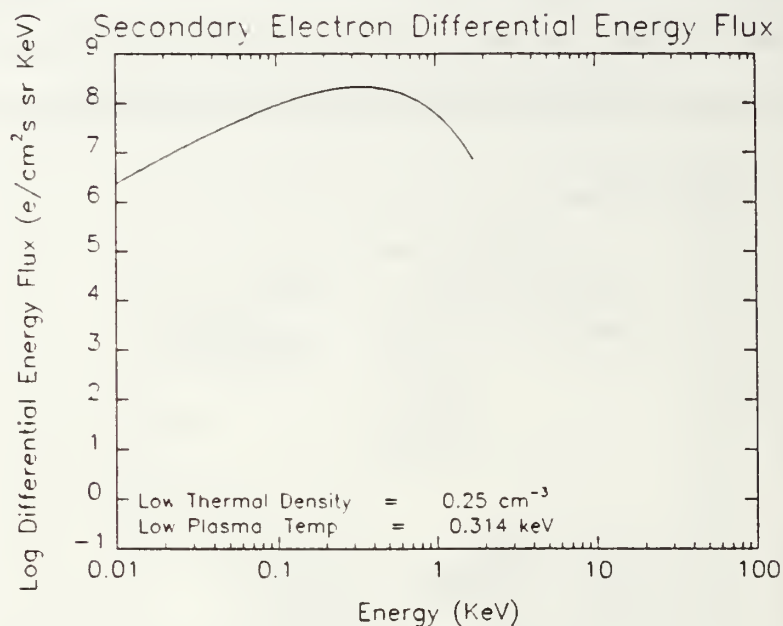Log Differential Energy Flux (e/cm^{2}s sr KeV)

Figure 27

The majority of the electrons emitted result from the

differential energy flux below approximately 2 keV. This is

because the peak of the secondary yield curve is between 300

64

and 400 eV. This corresponds to the peak in the low energy segment of the incident flux (Figure 26). The flux due to secondary emission is higher than the ambient flux. For 0 to 1.5 keV, the peak incident flux is 1×10^8 e/(cm² s sr keV) and the peak outgoing secondary flux is 4×10^8 e/(cm² s sr keV).

This reflects the fact that the low energy segment of the differential energy flux is between the first and second crossover energies for this satellite material, as seen in Figure 17. This shows that for low energy electrons in the ambient differential energy flux incident onto the spacecraft surface, the secondary yield differential energy flux over-balances the incident flux.

3. Backscattered Differential Energy Flux

The backscattered differential energy flux is directly dependent on the incident ambient differential energy flux. The particles that are emitted from the satellite surface below 50 eV are included in the calculation of the secondary yield differential energy flux. The two Maxwellian components to the distribution function both contribute to backscattered electron flux. Figure 28 shows the backscattered differential energy flux, as a function of energy, for the ISEE 1 spectrum. The backscatter flux is an order of magnitude below the ambient differential energy flux. The peaks in the backscatter

curve correspond with the peaks in the incident spectrum because the yield curve is relative flat. The net effect of backscattering is to reduce the net current due to the ambient (0 to 40 keV) electrons by a factor of 10% to 20%.
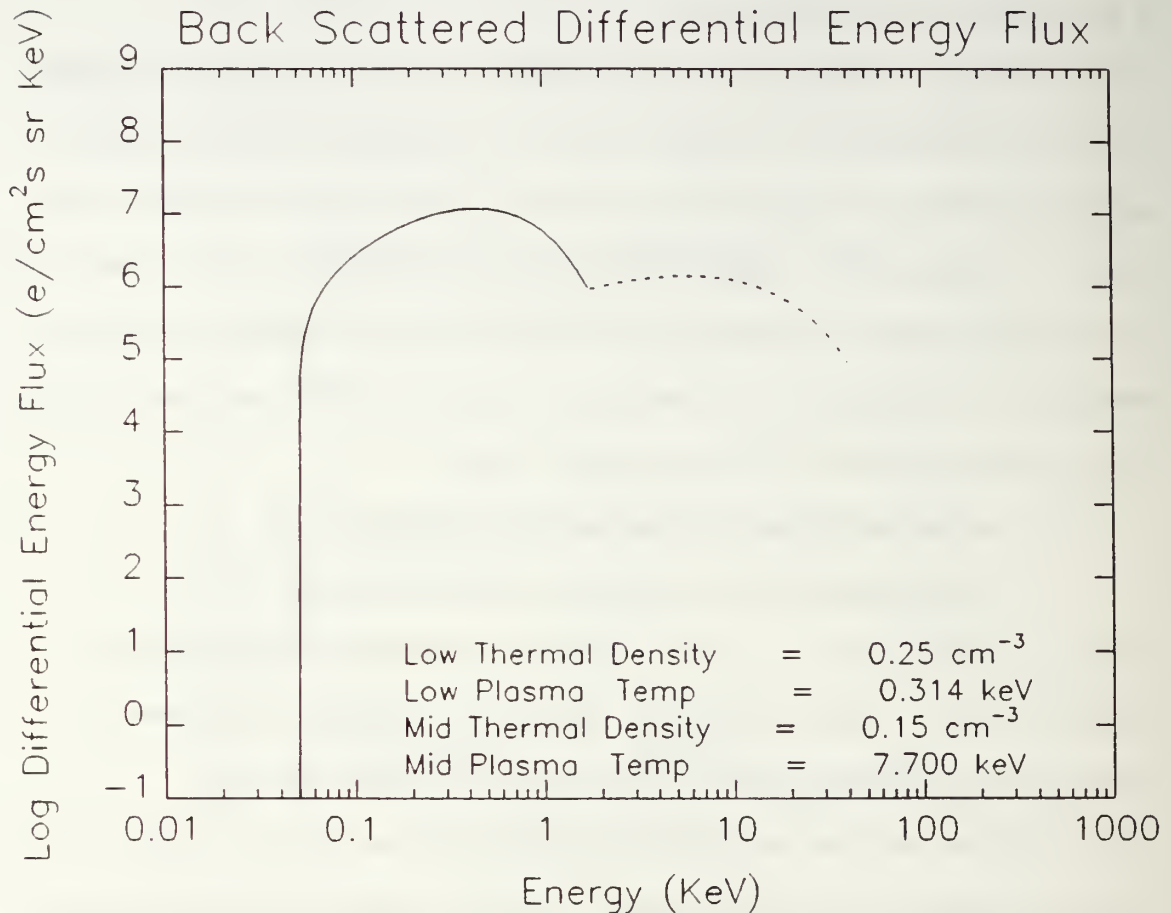

Figure 28

For more energetic electrons, the influence of surface atom interaction will decrease and they will be more likely to bury themselves into dielectric surfaces, as shown

in Figure 22. The remaining calculations, therefore, are associated with correctly determining the deposited charge. To do this we need to determine the radiation-induced conductivity.

4. Radiation-Induced Conductivity

Incident solar radiation onto dielectric materials on spacecraft surfaces will, over time, cause the RIC of the surface to change. The change in conductivity directly effects the rate at which charge that enters the dielectric material when energetic electrons bury themselves, leaks out. This, in turn, helps determine whether enough charge can build up in the dielectric to surpass the dielectric breakdown threshold and cause an electrical discharge. The energetic portion of the differential energy flux is shown in Figure 29, in units of $e/(cm^2 \, s \, MeV)$, from 10 to 200 keV.

Calculation of RIC requires a calculation of dose. This is done by convolving the energetic current density, $J(E)$, the collisional stopping power (Figure 23), and the specific thickness curve (Figure 24) to obtain the differential dose rate $(gm \, sec)^{-1}$. Integrating the differential dose rate from 10 to 450 keV gives the dose rate in $MeV/(gm \, sec)$. Figure 30 shows a graph of the penetration depth, in cm, of energetic electrons as a function of the incident dose rate.
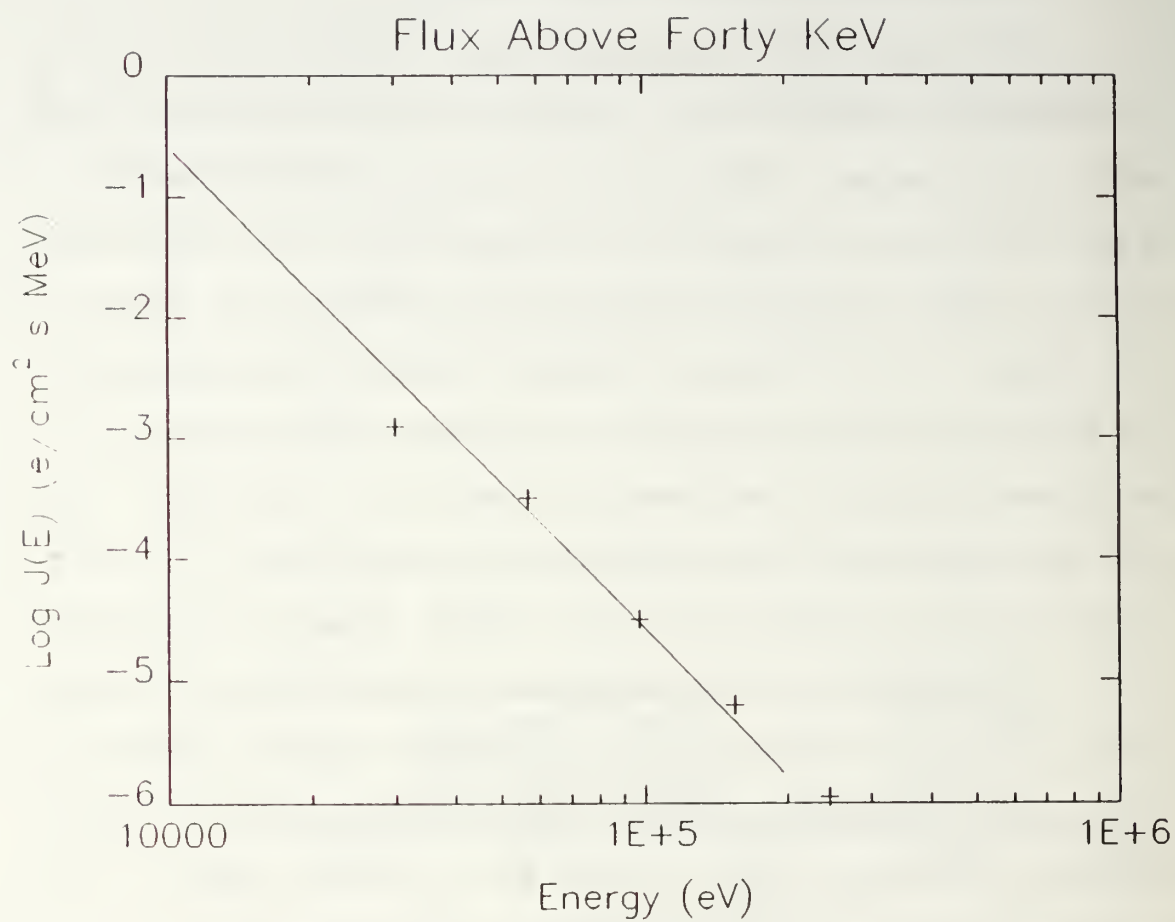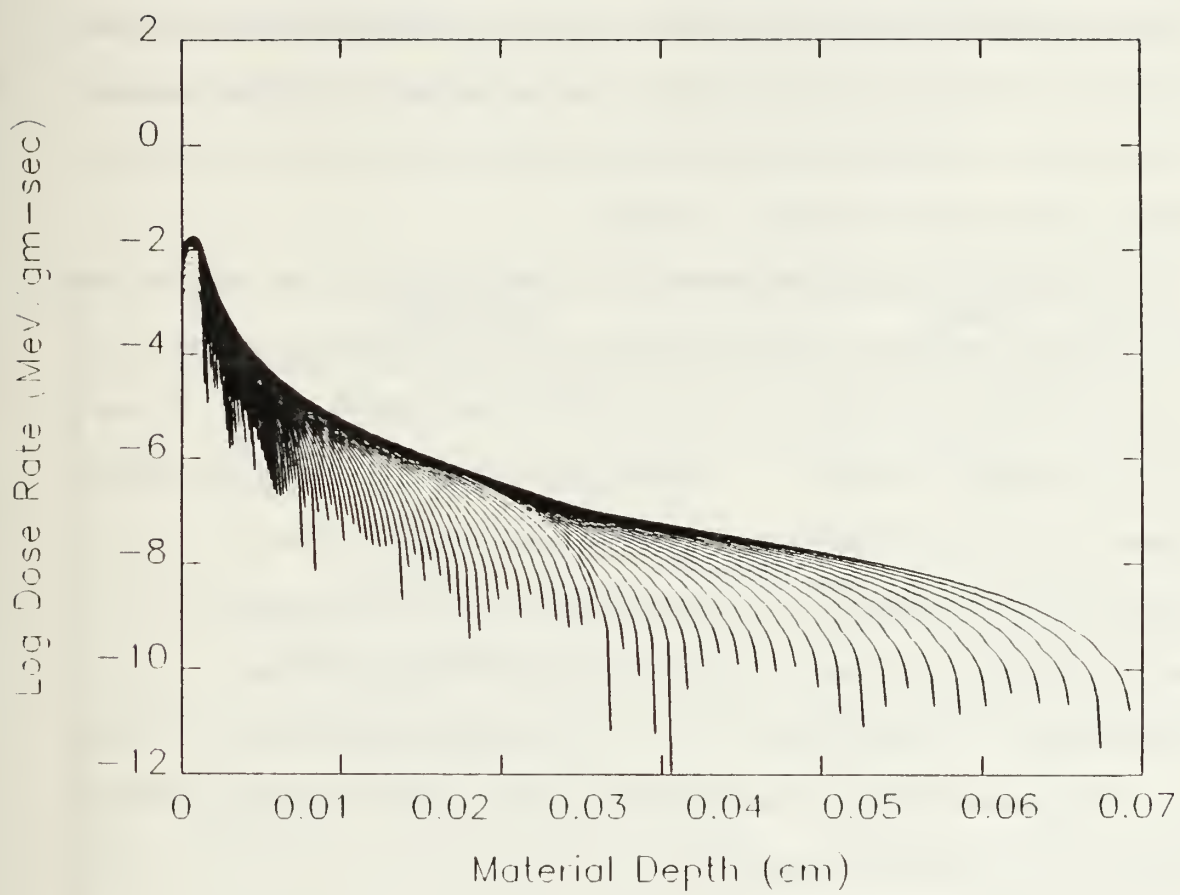
Figure 29

68

Figure 30

69

The figure shows an overlay of different energies and how far into the dielectric material they penetrate. The lowest energy was 10 keV and the highest was 450 keV. The dielectric material used for this graph was borosilicate glass. An upper bound of 230 keV was used as it is the maximum energy incident onto a .03 cm solar array cover cell that will deposit itself into the material. Higher energy electrons will pass through the cover cells and into the body of the spacecraft.

The integrated dose rate for the 0.03 cm dielectric, is ~ 0.06 rad/sec. Multiplying this dose rate by the largest value in table 5 (k_{max} = 10^{-16} sec/(Ω cm rad) gives σ_{RIC} = 6 x 10^{-18} (Ω cm)$^{-1}$. The value of σ_i for Corning 7940 glass is 1 x 10^{-15} (Ω cm)$^{-1}$ [Ref 41, p. 141]. The conductivity change from radiation is ~ two orders of magnitude below the intrinsic conductivity of the dielectric. This shows that RIC is an minor factor in the overall deposition of charge and, for the purposes of this thesis, RIC can be ignored.

5. **Surface Charge**

The distribution function for day 76, as shown in Figure 25, was used to calculate the flux components through the satellite surface. Table 6 shows the flux components and their respective contributions to the net flux. The table is organized as follows. The ambient flux is divided

70

into three components, the low, mid, and energetic energies.
Summing each contribution gives the incident flux.   That
flux which is produced from secondary emission is labelled
secondary flux.   The backscatter flux is made up of two
components, the low and mid energy fluxes.   The net flux is
the incident flux minus the sum of the secondary and
backscattered fluxes.

COMPONENT	e/m^2 s x 10^{11}
Flux < 1.7 keV	7.24
Flux > 1.7 keV & < 40 keV	20.76
Flux > 40 keV	1.39
Total Incident Flux	29.4
Secondary Flux	15.9
BS Flux > .05 keV & <1.7 keV	.65
BS Flux > 1.7 keV & < 40 keV	2.53
Total BS Flux	3.18
Net Flux	10.3

The ambient current is .47 $\mu A/m^2$.   The energetic
flux alone contributes a current density of 0.022 $\mu A/m^2$, a

very small part of the total. Combining the secondary and backscatter fluxes gives the amount of flux that leaves the surface. The current density J leaving the surface is $J_{backscatter + secondary}$, = .306 $\mu A/m^2$. The net current due to the ambient electrons is approximately 0.16 $\mu A/m^2$ negative. Hence, a glass surface in shadow should charge negatively. The photoelectric saturation current density from Table 4 is nominally 21 $\mu A/m^2$. This shows that when the satellite is in sunlight, the current density from incident photons is two orders of magnitude higher than the current due to the plasma. Therefore, whenever the satellite is in sunlight, the amount of charge that leaves the surface is greater than that deposited, and the potential of the vehicle should be positive.

If we make the assumption that the satellite exits the midnight to dawn sector with a vehicle potential close to zero, then the potential will become positive from photoelectric emission in the absence of a warm/hot plasma. The ISEE 1 period of rotation is three seconds. This means that while in sunlight, approximately 20% to 25% of the vehicle is in sunlight. Using equation (24) and a spin period of three seconds, a net charge of 12.7 $\mu C/m^2$ leaves the spacecraft surface each period. This effect dominates the other mechanisms and is responsible for maintaining the potential close to zero in the absence of an energetic plasma.

6. Deep Dielectric Charge

There is an additional aspect of the charging process that must be considered. Energetic electrons of a few keV and above began to bury themselves into the body of the dielectric, where they become trapped. This buildup of charge within the dielectric can develop over an extended period of time, and the associated electric fields may surpass the breakdown dielectric strength, typically on the order of 10^6 V/cm [Ref 34, p. 569 to 591]. For a 0.03 cm cover cell, the potential threshold can be as low as 3000 volts negative, but is more likely to be higher. This has been the focus of previous studies of deep dielectric charging such as the one by Reagan [Ref 21]. This charge deposition has another consequence, however.

Consider the time for the spacecraft to move through the eclipse to be one hour. The deposited charge which results from the "energetic" portion of the spectrum depends on the lower limit in the integration of J(E) over E. Previous work at the Naval Postgraduate School focused on $E_{min} = 100$ keV. If the lower limit is reduced, a wider energy range is included in the integration. This substantially increases the energetic current, and hence the deposited charge.

Figure 31 shows J(E) integrated over energy from E_{min} to infinity. The data used for the calculation are from

Figure 26. Again, ISEE 1 was passing through geosynchronous altitude at 0300 LT [Ref 13]. By varying the lower limit of integration, the current density inversely increases. The vertical axis is the result of q x ∫ J(E) dE. As you might expect, the bulk of the current contribution comes at the low end of the energy spectrum.
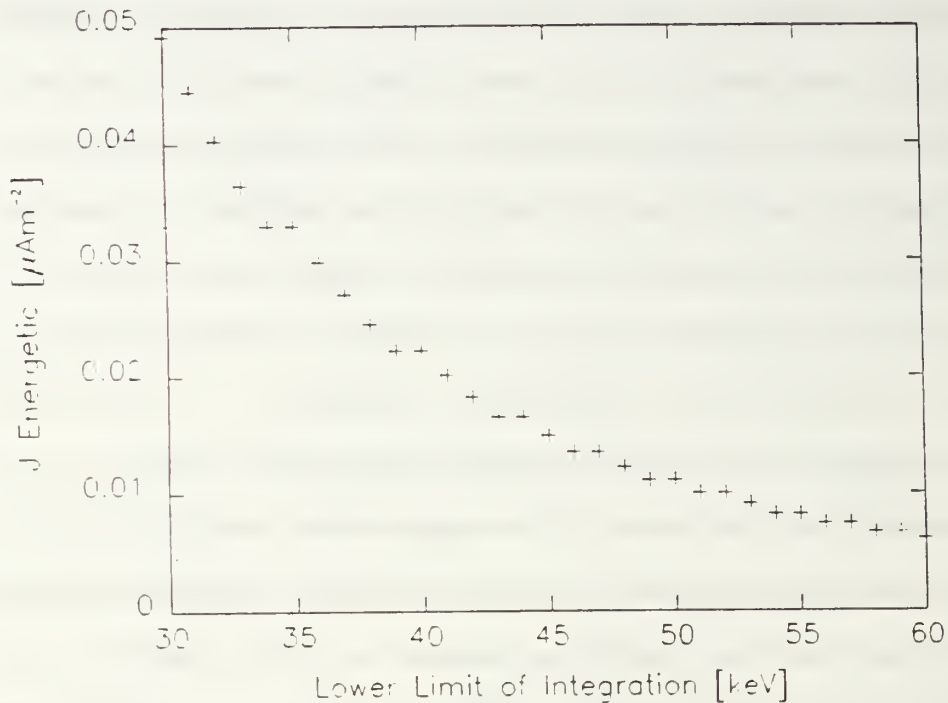

Figure 31

The question, then, is how much charge can be deposited over the period of interest. Figure 31 determines the time period for the ISEE 1 satellite to charge via our proposed mechanism. Conversely, taking one hour as the period, then the charge is proportional to the flux and will

range from ~ 180 $\mu C/m^2$ down to ~ 20 $\mu C/m^2$. These numbers
are comparable to, or larger, than the net charge which is
emitted as a result of photoemission in a spin period. This
differs substantially from the previous result [Ref 23]
where the low energy limit was 100 keV. This shows that the
recommendation for further calculations at lower energies
was correct. Note that the energy range (10 to 30 keV) not
included here, will also contribute, though surface
conductivity will render these less deeply buried electrons
ineffective for long time scale processes. The inequality
in equation (24) is satisfied, indicating that the mechanism
proposed for the development of differential charge on ISEE
1 satellite should be viable.

The ISEE 1 charging event was nearly unique for this
vehicle. The reason appears to be that the energetic
electron flux was relatively high on this day. Data from a
second satellite provides selected examples of events with
very high fluxes of energetic electrons.

B.   SCATHA

Reagan et al., surveyed the near-geosynchronous SCATHA
data set and identified the peak energetic flux events [Ref
21]. Figure 32 shows all of these high flux days. One of
these large events was on 29 August, 1979. The data was
recorded by the P78-2 SCATHA satellite, which was at 6.5 R_E,
in sunlight, and at 0230 LT. The differential flux, as

shown in Figure 32 for day 241a, was used here. This
energetic plasma was then compared to day 76. The energetic
current density integrated from 40 keV to 1 MeV gives
$J_{energetic} = 0.235$ $\mu A/m^2$. Figure 33 shows the calculations for
$J_{energetic}$. The energetic plasma of day 241a provided 5 times
more current than observed on ISEE 1. Such fluxes would
cause substantial charge deposition in 5 to 10 minutes.

This implies that although high, the ISEE 1 fluxes were
not record setting, and that deep dielectric charging could
become important on a time scale of ~ 10 minutes. Note that
on day 241a, the electron flux is very high from 4 to 40
keV. This energy range is responsible for both deep
dielectric charging and subsequent surface charging in the
SCATHA survey. Figure 34 shows the SCATHA potential on day
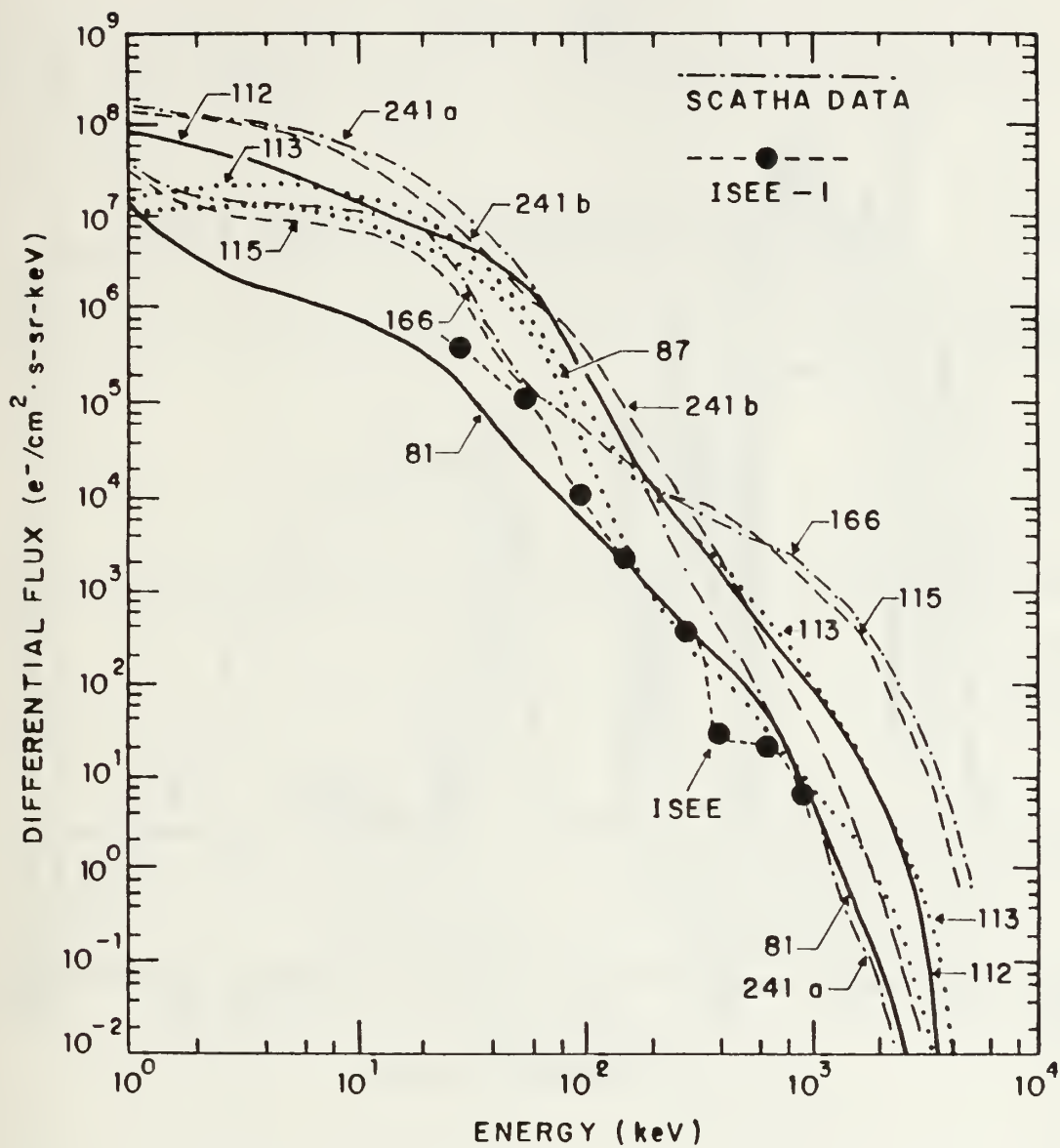241a plotted against time. This event was one of largest
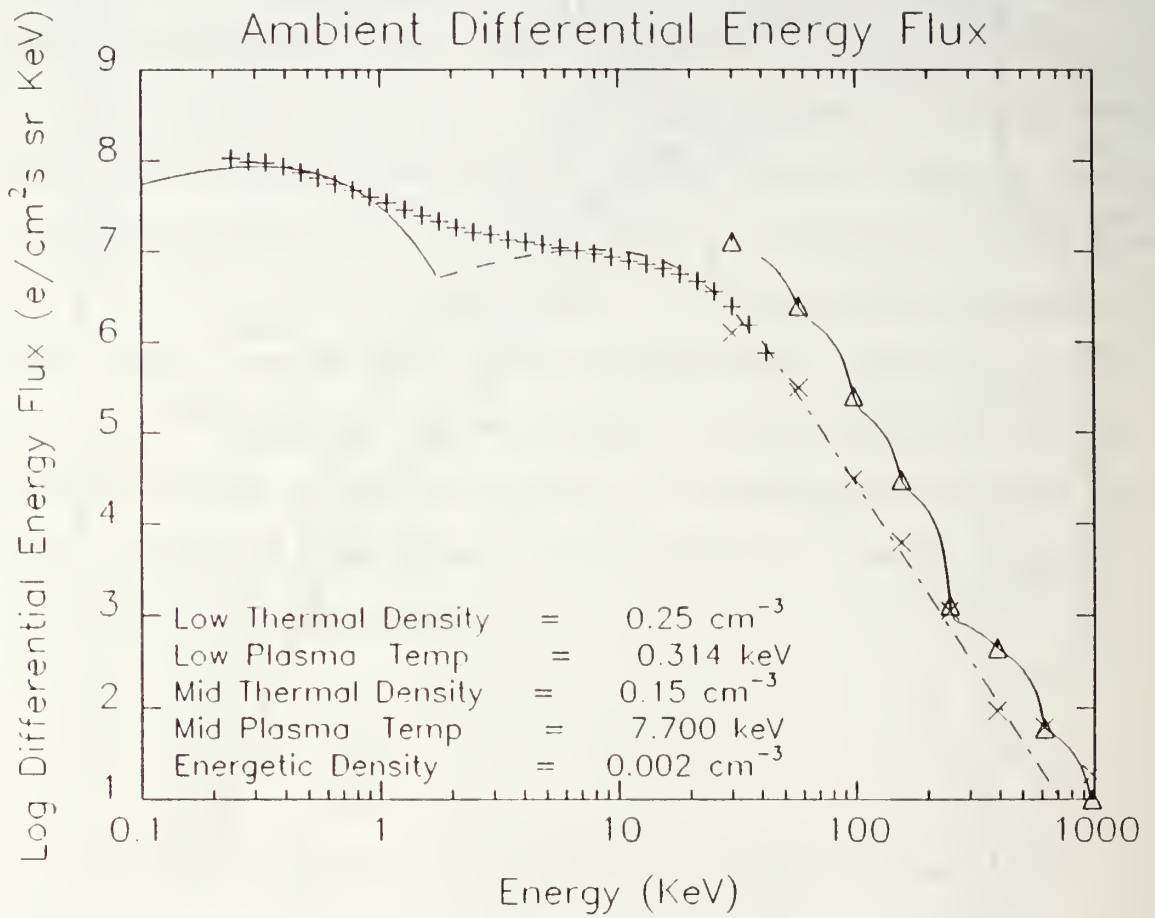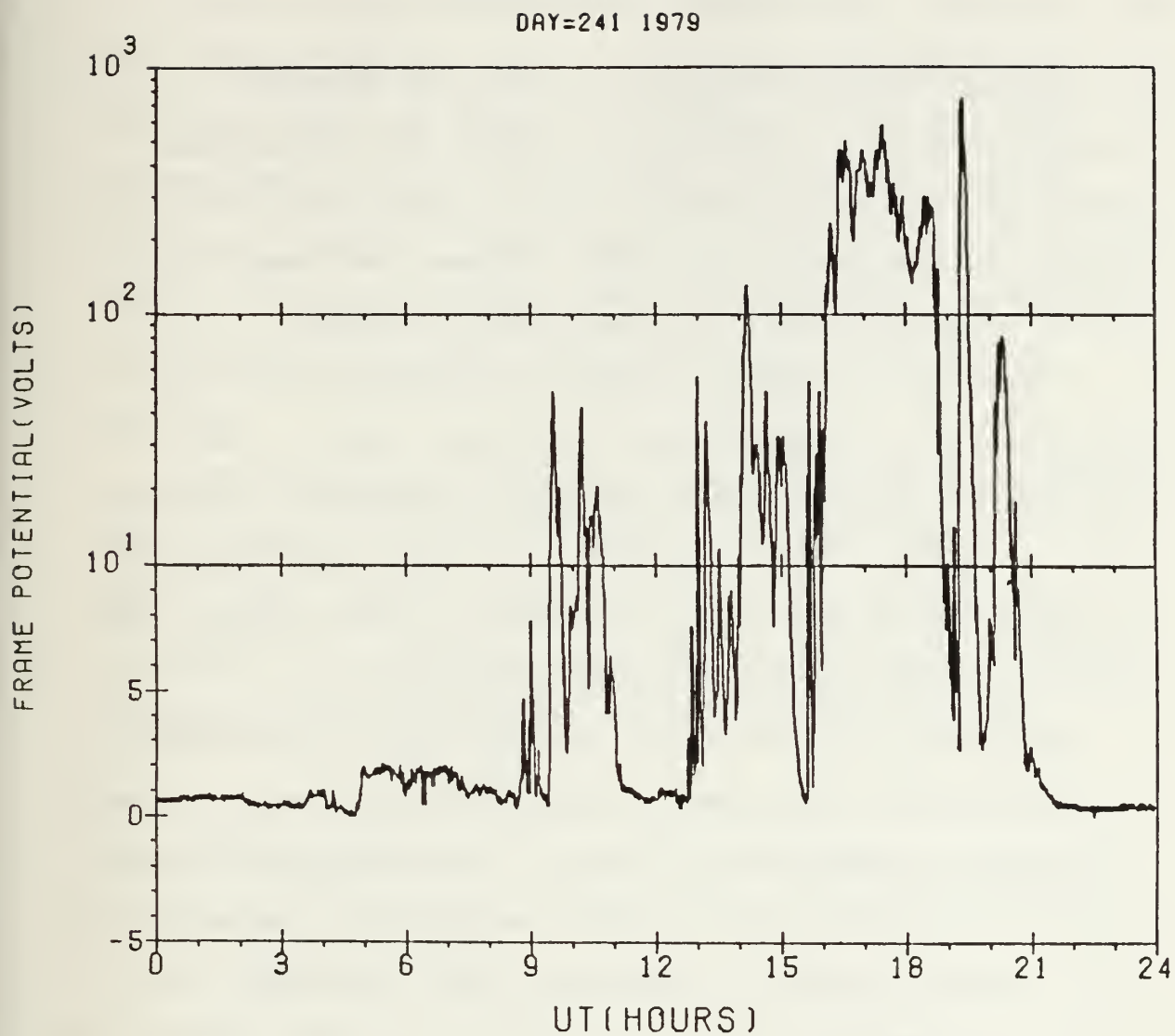recorded on SCATHA.

Figure 32

[Ref 21]

Figure 33

78

DAY=241 1979

Figure 34

[Ref 12]

V. CONCLUSIONS

Spacecraft at geosynchronous altitude encounter energetic plasmas as they move through the plasmasheet. These hot plasmas can effect satellite functions. EMPs induced in spacecraft electrical systems can cause data upsets, system resets, and even system failures.

Traditional charging studies focused on the nearly instantaneous processes found in eclipse [Ref 7], and daylight charging processes with time constants of minutes [Ref 17, Ref 8]. This work has shown that deep dielectric charging, which occurs on time scales of many minutes, may also be significant for daylight charging.

Deep dielectric charging, occurs when the distribution function of the hot plasma contains electrons whose average temperature exceeds about 10 keV. This mechanism deposits energetic electrons deep within the dielectric materials on the satellite surface. The charge deposited within the dielectric remains stationary, leaking out over a period of many hours. This buildup of charge within the dielectrics is independent of the other processes involving the surface.

The critical question is, if more charge can be deposited in an hour or less than emitted from the surface

in one spin of the satellite, will an isolated segment of dielectric develop a net negative charge?

Records from very energetic plasmas were examined. Data from ISEE 1 daylight negative potential event and the record daylight event for SCATHA were studied. The ISEE data showed that if 40 to 250 keV electrons are considered, sufficient charge is deposited in an hour to result in a net negative charge. The five times higher fluxes observed on SCATHA would reduce the charging time scale to a few minutes.

Deep dielectric charging is important and may determine the daylight potential behavior of geosynchronous satellites. In particular, it may provide a charging mechanism for rapidly spinning satellites, which do not otherwise have the tendency to differentially charge.

VI. RECOMMENDATIONS

Follow up work should focus on the mechanism by which 10 keV to 200 keV electrons bury themselves into dielectric materials. Modelling of the process would produce numerical values that should be compared to recorded charging events and the attendant electron distribution function. The speculation that deep dielectric charging will lead to daylight negative potentials needs to be studied via modelling.

LIST OF REFERENCES

1. Robinson Jr., P. A., "Spacecraft Environmental Anomalies Handbook", Jet Propulsion Laboratory, California Institute of Technology, August, 1989, for Geophysics Laboratory, Hanscom AFB, Massachusetts.

2. McIlwain, C. E., Coordinates for mapping the distribution of magnetically-trapped particles, Journal of Geophysical Research, vol. 66, 1961.

3. Parks, G. K., "Physics of Space Plasmas", Addison-Wesley Publishing Company, 1991.

4. Deforest, S. and McIlwain, C. E., Plasma Clouds in the Magnetosphere, Journal Of Geophysical Research, vol. 76, 1971.

5. Fredricks, R. W. and Scarf, F. L., Observations of Spacecraft Charging Effects in Energetic Plasma Regions, Proceedings of the 6th ESLAB Symposium, Noordwijk, The Netherlands, edited by R. J. L. Grard, 26 - 29 September, 1972.

6. Baker, D. N., et al, Hostile Energetic Particle Radiation Environments in Earth's Outer Magnetosphere, The Aerospace Environment at High Altitudes and its Implications for Spacecraft Charging and Communications, AGARD Conference Proceedings No. 406, The Hague, The Netherlands, 1986.

7. Deforest, S.E., Spacecraft Charging at Synchronous Orbits, Journal of Geophysical Research, vol. 77, 1972.

8. Olsen, R. C., and Purvis, C. K., Observations of Charging Dynamics, Journal of Geophysical Research, vol. 88, 1983.

9. Deforest, S. E., Electrostatic Potentials Developed by ATS-5, Photon and Particle Interactions with Surfaces in Space, Proceedings of the 6th ESLAB Symposium, Noordwijk, The Netherlands, edited by R. J. L. Grard, 26 - 29 September, 1972.

10. Olsen, R. C., Record Charging Events from Applied Technology Satellite 6, Journal of Spacecraft and Rockets, Vol. 24, 1987.

11. Reasoner, D. L. et al., Relationship Between ATS-6 Spacecraft-Charging Occurrences and Warm Plasma Encounters, Progress in Astronautics and Aeronautics, edited by A. Rosen, vol. 47, 1976.

12. Mullen, E. G. et al, SCATHA Survey of High-Level Spacecraft Charging in Sunlight, Journal Of Geophysical research, Vol. 91, 1986.

13. Olsen, R. C. and Whipple, E. C., An Unusual Charging Event on ISEE I, Journal of Geophysical Research, vol. 93, 1988.

14. Frooninckx, T. B. and Sojka, J. J., Solar Cycle Dependence of Spacecraft Charging in LEO, Journal of Geophysical Research, 1991.

15. Whipple Jr., E. C., Observation of Photoelectrons and Secondary Electrons Reflected from a Potential Barrier in the Vicinity of ATS 6, Journal of Geophysical Research, vol. 81, 1976.

16. Olsen, R. C. et al, Observation of Dynamic Charging Effects on ATS 6, Journal of Geophysical Research, Vol. 86, 1981.

17. Katz, I. et al., Secondary Electron generation, Emission and Transport: Effects on Spacecraft Charging and NASCAP Models, The Aerospace Environment at High Altitudes and its Implications for Spacecraft Charging and Communications, AGARD Conference Proceedings No. 406, The Hague, The Netherlands, 1986.

18. Mizera, P. F., Charging Results from the Satellite Surface Potential Monitor, Journal of Spacecraft, vol. 18, no. 6, 1980.

19. Koons, H. C. et al, Severe Spacecraft charging Event on SCATHA in September 1982, Journal of Spacecraft, vol. 18, no. 6, 1980.

20. Vampola, A. L., Thick Dielectric Charging on High-Altitude Spacecraft, Journal of Electrostatics, vol. 20, 1987.

21. Reagan, J. B. et al, Space Charging Currents and Their Effects on Spacecraft Systems, IEEE Transactions of Electrical Insulation, vol. EI-18, June, 1983.

22. Olsen, R.C., private communication.

23. Young, M. E., Dielectric Charging as a Catalyst to the Formation of Potential Barriers on Synchronous Orbit Satellites, Master's Thesis, Naval Postgraduate School, Monterey, California, March, 1990.

24. Garrett, H. B., Spacecraft Charging: A Review, Progress in Astronautics and Aeronautics, vol. 71, 1980.

25. Olsen, R. C., Differential and Active Charging Results from the ATS Spacecraft, Ph.D. Dissertation, University of California, San Diego, San Diego, California, 1980.

26. Olsen, R. C., A Threshold Effect for Spacecraft Charging, Journal of Geophysical Research, vol. 88, 1983.

27. Sternglass, E. J., Secondary Electron Emission and Atomic Shell Structure, Physics Review, No. 80, 1950.

28. Katz, I et al., A Three Dimensional Dynamic Study of Electrostatic Charging in Materials, NASA CR-135256, SSS-R-77-3367, 1977.

29. Darlington, E. H. and Cosslett, V. E., Backscattering of 0.5 - 10 keV Electrons from solid targets, J Physical D: Applied Physics, vol. 5, 1972.

30. Grard, R. J. L., Knott, K., and Pedersen, A., The influence of Photoelectron and Secondary Electron Emission on Electric Field Measurements in the Magnetosphere and Solar Wind, Proceedings of the 6th ESLAB Symposium, Noordwijk, The Netherlands, edited by R. J. L. Grard, 26 - 29 September, 1972.

31. Whipple, E. C., The Equilibrium Electric Potential of a Body in the Upper Atmosphere and in Interplanetary Space, Ph.D. Dissertation, George Washington University, Washington, D.C., June, 1965.

32. Rudie, N. J., Principles and Techniques of Radiation Hardening, vol. I, Western Periodicals Company, 1986.

33. Wenaas, E. P., Spacecraft Charging Effects by the High-Energy Natural Environment, IEEE Transactions on Nuclear Science, vol. 24, 1977.

34. Wall, J. A., et al., Results of Literature Search on Dielectric Properties and Electron Interaction Phenomena Related to Spacecraft Charging, Proceedings of the Spacecraft Charging Technology Conference, edited by Pike, C. P. and Lovell, R. R., AFGL-TR-77-0051, 1977.

35. Berger, M. J. and Seltzer, S. M., Stopping Powers and Ranges of Electrons and Positrons (2nd Ed.), U. S. Department of Commerce, NSBIR 82-2550-A, 1982.

36. Meulenberg Jr., A. Evidence for a New Discharge Mechanism for Dielectrics in a Plasma, Progress in Astronautics and Aeronautics, vol. 47, 1976.

37. Frederickson, D. B. et al., Spacecraft Dielectric Material Properties and Spacecraft Charging, Progress in Astronautics and Aeronautics, M. Summerfield, Series Editor-in-Chief, vol. 107, 1986.

38. Olsen, R. C., Modification of Spacecraft Potentials by Thermal Electron Emission on ATS-5, Journal of Spacecraft and Rockets, Vol. 16, no. 6, 1981.

39. Lai, S. T. et al., The Concepts of Critical Temperature and Energy Cutoff of Ambient Electrons in High Voltage Charging of Spacecraft, Proceedings of the 6th ESLAB Symposium, Noordwijk, The Netherlands, edited by R. J. L. Grard, 26 - 29 September, 1972.

40. Olsen, R. C., McIlwain, C. E., and Whipple, Jr., E. C., Observations of Differential Charging on ATS 6, Journal of Geophysical Research, vol. 86, 1981.

41. Reitz, J. R., Milford, F. J., and Christy, R. W., Foundations of Electromagnetic Theory, Addison-Wesley, 1980.

INITIAL DISTRIBUTION LIST

1. Defense Technical Information Center   2
   Cameron Station
   Alexandria, Virginia 22304-6145

2. Commandant of the Marine Corps   1
   Code TE 06
   Headquarters, U.S. Marine Corps
   Washington, D. C. 20380-0001

3. Superintendent   2
   Attn: Library, Code 52
   Naval Postgraduate School
   Monterey, California 93943-5000

4. Department Chairman, Code PH   1
   Department of Physics
   Naval Postgraduate School
   Monterey, California 93943-5000

5. Dr. R. C. Olsen, Code PH/OS   4
   Department of Physics
   Naval Postgraduate School
   Monterey, California 93943-5000

6. Dr. X. K. Maruyama, Code 61MX   1
   Department of Physics
   Naval Postgraduate School
   Monterey, California 93943-5000

7. Capt. D. S. Smith   2
   P.O. Box 8152
   Truckee, California 96162-8152

8. Dr. E. C. Whipple   1
   NASA/HQ 155
   Washington, D. C. 20546

9. Mr. Gracen Joiner   1
   Code 1114 Sp
   Office of Naval Research
   800 N. Quincy Street
   Arlington, Virginia 22217